JACS
JOURNAL OF THE AMERICAN CHEMICAL SOCIETY

Article

pubs.acs.org/JACS

Thermodynamic and Kinetic Study of Cleavage of the N−O Bond of N-Oxides by a Vanadium(III) Complex: Enhanced Oxygen Atom Transfer Reaction Rates for Adducts of Nitrous Oxide and Mesityl Nitrile Oxide

Taryn D. Palluccio,[†] Elena V. Rybak-Akimova,*[,†] Subhojit Majumdar,[‡] Xiaochen Cai,[‡] Megan Chui,[‡] Manuel Temprado,*[,§] Jared S. Silvia,[∥] Anthony F. Cozzolino,[∥] Daniel Tofan,[∥] Alexandra Velian,[∥] Christopher C. Cummins,*[,∥] Burjor Captain,*[,‡] and Carl D. Hoff*[,‡]

[†]Department of Chemistry, Tufts University, 62 Talbot Avenue, Medford, Massachusetts 02155, United States

[‡]Department of Chemistry, University of Miami, 1301 Memorial Drive, Coral Gables, Florida 33021, United States

[§]Department of Physical Chemistry, Universidad de Alcalá, Ctra. Madrid-Barcelona Km. 33,600, Madrid 28871, Spain

[∥]Department of Chemistry, Massachusetts Institute of Technology, 77 Massachusetts Avenue, Cambridge, Massachusetts 02139, United States

Supporting Information

ABSTRACT: Thermodynamic, kinetic, and computational studies are reported for oxygen atom transfer (OAT) to the complex $V(N[t\text{-Bu}]Ar)_3$ (Ar = 3,5-$C_6H_3Me_2$, **1**) from compounds containing N−O bonds with a range of BDEs spanning nearly 100 kcal mol^{-1}: PhNO (108) > SIPr/MesCNO (75) > PyO (63) > IPr/N_2O (62) > MesCNO (53) > N_2O (40) > dbabhNO (10) (Mes = mesityl; SIPr = 1,3-bis(diisopropyl)-phenylimidazolin-2-ylidene; Py = pyridine; IPr = 1,3-bis(diisopropyl)phenylimidazol-2-ylidene; dbabh = 2,3:5,6-dibenzo-7-azabicyclo[2.2.1]hepta-2,5-diene). Stopped flow kinetic studies of the OAT reactions show a range of kinetic behavior influenced by both the mode and strength of coordination of the O donor and its ease of atom transfer. Four categories of kinetic behavior are observed depending upon the magnitudes of the rate constants involved: (I) dinuclear OAT following an overall third order rate law (N_2O); (II) formation of stable oxidant-bound complexes followed by OAT in a separate step (PyO and PhNO); (III) transient formation and decay of metastable oxidant-bound intermediates on the same time scale as OAT (SIPr/MesCNO and IPr/N_2O); (IV) steady-state kinetics in which no detectable intermediates are observed (dbabhNO and MesCNO). Thermochemical studies of OAT to **1** show that the V−O bond in $O{\equiv}V(N[t\text{-Bu}]Ar)_3$ is strong (BDE = 154 ± 3 kcal mol^{-1}) compared with all the N−O bonds cleaved. In contrast, measurement of the N−O bond in dbabhNO show it to be especially weak (BDE = 10 ± 3 kcal mol^{-1}) and that dissociation of dbabhNO to anthracene, N_2, and a ^{3}O atom is thermodynamically favorable at room temperature. Comparison of the OAT of adducts of N_2O and MesCNO to the bulky complex **1** show a faster rate than in the case of free N_2O or MesCNO despite increased steric hindrance of the adducts.

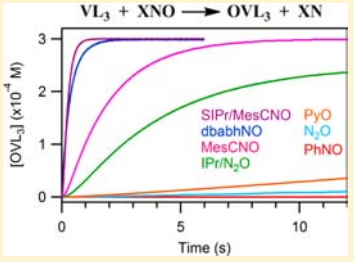

1. INTRODUCTION

Oxygen atom transfer (OAT)[1] involving nitrogen oxides (XNO) reacting with metal complexes is of fundamental importance to developing catalytic oxidation chemistry for the most abundant pnictogen. In particular, N_2O is a significant greenhouse gas which is three hundred times more potent than CO_2 as a pollutant.[2] It is a byproduct of several industrial processes[3] making its utilization of economic and environmental significance. A barrier to that is the relatively inert nature of N_2O as an oxidant.[4] Since the pioneering work of Taube and Armor[5] showing that oxidation of Cr^{2+} by N_2O is accelerated by a factor of 10^8 when it is complexed to $Ru(NH_3)_5^{2+}$, a number of studies have focused on whether oxidation by N_2O occurs by initial coordination through the terminal O or terminal N atom of the ligand. Recently Lin et al.[6] have performed computational studies and concluded that OAT reactions of N_2O to middle transition metal complexes occur faster by initial N coordination to form a nitrosoimide complex $L_nM{=}N{-}N{=}O$, which then undergoes an essentially barrierless OAT to a second equivalent of metal complex leading to overall third-order reactivity. Caulton and co-workers[7] had earlier performed computational studies in which novel modes of coordination of N_2O were proposed, including that of a nitrosoimido resembling that formulated by Lin et al.[6] Despite considerable interest in nitrous oxide complex chemistry, the first structure of bound N_2O was reported only recently and did not correspond to a nitrosoimide binding motif.[8] There are relatively few experimental kinetic studies of OAT from N_2O to metal complexes in solution,[9] and the authors could find no

Received: May 29, 2013
Published: June 27, 2013

   dx.doi.org/10.1021/ja405395z | J. Am. Chem. Soc. 2013, 135, 11357−11372

examples of third-order kinetics implying a ternary transition state. Detailed kinetic, thermodynamic, and computational studies of the reaction of $Mo(N[t\text{-}Bu]Ar)_3$ with N_2O, which results in cleavage of the N−N rather than the N−O bond to yield $N{\equiv}Mo(N[t\text{-}Bu]Ar)_3$ and $ON{-}Mo(N[t\text{-}Bu]Ar)_3$, have been reported earlier.[10]

While nitrous oxide represents an important substrate, other nitrogen oxides are also of significance and generally require catalytic activation in OAT, the first step of which is transfer to an active metal complex.[11] A general two step mechanism involving initial oxidant binding followed by OAT is illustrated for XNO in eq 1.

$$ML_n + XNO \underset{k_{-1}}{\overset{k_1}{\rightleftharpoons}} XNO{-}ML_n \overset{k_2}{\rightarrow} XN + OML_n \quad (1)$$

The mechanism shown in eq 1 is deceptively simple. Portrayal of a general $XNO{-}ML_n$ adduct hides the fact that the nature of the intermediate formed can undergo significant change as the X group is varied and important aspects of spin state, bond strength, charge transfer, and adduct geometry are not displayed. These factors will all show up in the magnitudes of the various rate constants involved as X is changed.

A number of benchmark studies have been made in metal-mediated OAT, though results from one system can be extrapolated to another only with considerable risk. Pioneering work by Schultz and Holm[12] for OAT cycling between $L_2Mo(IV)(O)$ and $L_2Mo(VI)(O)_2$ showed that rates of OAT spanned 4 orders of magnitude. In some cases, there was good correlation between the rates of OAT and the BDE of the bond being broken, but the substrate with the largest BDE studied, Ph_3AsO (103 kcal mol^{-1}), had an activation energy the same as that for the one with the smallest BDE, Ph_2SeO (43 kcal mol^{-1}). Recent work by Abu-Omar[13] has shown the importance of both binding, the first step in OAT, and the actual OAT reaction in the second step. The importance of symmetry and geometry as well as electronic factors in OAT to $M(silox)_3$ complexes has been delineated by Wolczanski, Cundari, and co-workers[14] where the importance of achieving a nonlinear transition state was emphasized. Mayer and co-workers[15] have examined the effects of spin-state change on gas-phase OAT to Cr(III) porphyrin complexes. Interestingly, they found that above a certain threshold bond strength, OAT in either direction did not occur. "Ultrafast" and "ultraslow" rates of OAT to late transition metal complexes have been studied by Brown and co-workers.[16] Vasbinder and Espenson have shown that coordination of a second molecule of PyO (Py = pyridine) can serve to facilitate OAT of an already coordinated PyO ligand.[17] In addition to direct oxygen atom transfer, electron transfer followed by oxygen atom transfer has been studied by Fukuzumi and co-workers.[18] Detailed theoretical studies of OAT from metal oxo complexes to phosphines have been made by Hall and co-workers[19] which showed the importance of σ donation from the incoming phosphine to the $L_nM{=}O$ π^* orbital when the O atom is abstracted from the metal. Veige and co-workers[20] have recently shown that OAT from $Cr(V){\equiv}O$ to PR_3 is ~3000 times faster for PMe_3 than for $P(t\text{-}Bu)_3$ and is consistent with a bimolecular side-on attack at the $Cr(V){\equiv}O$ LUMO.

We have recently reported studies of OAT from mesityl nitrile oxide (MesCNO) to main group PX_n acceptors.[21] During that work the blue nitrile oxide−carbene adduct SIPr/MesCNO (SIPr = 1,3-bis(diisopropyl)phenylimidazolin-2-ylidene), in which the C atom of the N-heterocyclic carbene (NHC) is bound to the $C_{nitrile}$ atom of MesCNO, was isolated and structurally characterized. It was also found that formation of NHC adducts with the oxidant MesCNO suppressed oxygen atom transfer to main group elements. While reaction with Lewis bases was stopped by blocking attack at the $C_{nitrile}$ atom, qualitatively this was not observed to happen in reactions with the Lewis acid metal complex $V(N[t\text{-}Bu]Ar)_3$ (**1**), presumably since attack in this case occurred directly at the terminal O of MesCNO rather than at the interior $C_{nitrile}$ atom.

The initial goal of the current work was to quantitatively compare the rates of OAT to **1** from MesCNO and its NHC adduct SIPr/MesCNO simply to see which was faster. During this time, Severin and co-workers[22] reported characterization of stable covalent adducts of NHCs with N_2O and also showed that these adducts readily react with $V(Mes)_3$.[23] This prompted us to extend our work to compare N_2O and IPr/N_2O (IPr = 1,3-bis(diisopropyl) phenylimidazol-2-ylidene) and to study a series of XNO compounds with N−O bond dissociation enthalpies (BDEs) ranging from 10 to 108 kcal mol^{-1}, a range of nearly 100 kcal mol^{-1}. The N−O BDEs in the N-oxides studied are all significantly weaker than the V−O BDE in $O{\equiv}V(N[t\text{-}Bu]Ar)_3$ (**1**≡O, BDE = 154 kcal mol^{-1}), which makes N−O bond cleavage exothermic by 46 to 144 kcal mol^{-1}. While all bond cleavage reactions studied involve **1** and a N−O bond, a wide range of kinetic behavior was observed, allowing us to characterize individual reaction steps in detail.

2. EXPERIMENTAL SECTION

Detailed description of synthetic, solution calorimetric, stopped flow kinetic, and computational methods are provided in Supporting Information.

3. RESULTS

The main thrust of this paper is experimental mapping of the range of behavior of the OAT reactivity of nitrogen oxides with complex **1**. All XNO reagents studied (Scheme 1) were found

Scheme 1. (a) General Reaction Scheme of OAT to Complex 1 and (b) Structures of All the OAT Reagents Studied[a]

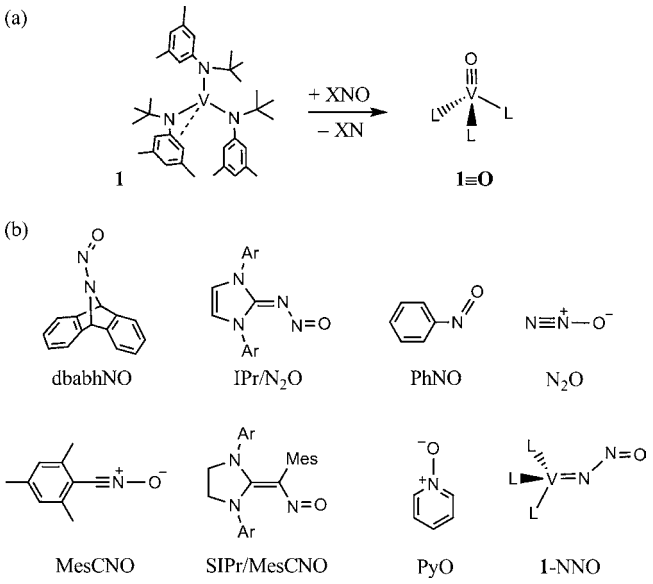

[a]L = N(*t*-Bu)Ar; Ar = 2,6-diisopropylphenyl; Mes = mesityl. Note that the $L_3V{=}N{-}N{=}O$ species is proposed, based on computational results, to be the precursor complex for dinuclear OAT from N_2O.

dx.doi.org/10.1021/ja405395z | J. Am. Chem. Soc. 2013, 135, 11357−11372

to react rapidly and cleanly at room temperature in toluene solution with paramagnetic complex **1** to produce the diamagnetic complex **1**≡O as confirmed by NMR spectroscopy. The experimental work is supported by theoretical calculations to provide more in depth analysis; however, full computational study of reaction mechanisms is beyond the scope of the current work. Such work is in progress and will be reported subsequently.[24] Following structural and thermochemical analysis, kinetic results are outlined.

3.1. Structural Analysis. *3.1.1. DFT-Calculated Structure of 1.* The structures of **1** and **1**≡O give insight into parameters influencing binding of oxidant and OAT reactivity in this system. To date, crystals of **1** suitable for X-ray structure determination have defied isolation. DFT computational studies, however, yield the minimum energy structure of **1** shown in Figure 1.

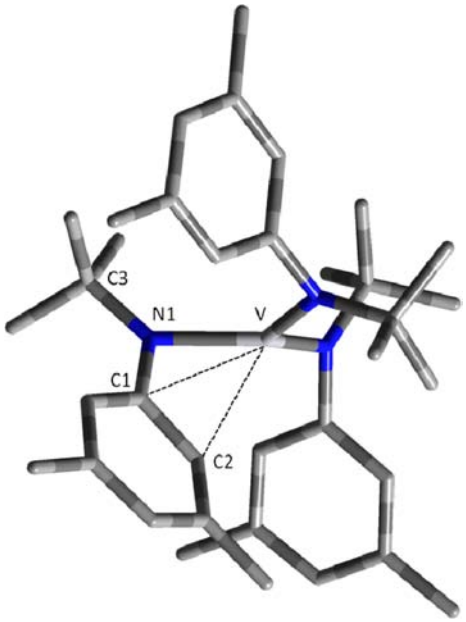

Figure 1. Optimized structure of **1** at the bp86/6-311G(d,p) (MDF10 for V with an additional set of f functions) level. Selected interatomic distances (Å) and angles (deg): V−C1 = 2.45; V−C2 = 2.42; V−N1−C1 = 92.1; V−N1−C3 = 138.3; C1−N1−C3 = 124.6; ∑(N−V−N) = 356.1.

The most stable configuration is a high-spin d^2 species exhibiting one close aryl contact through the single unoccupied d orbital (Figure 1). The same structural feature has been previously observed in the X-ray structure of the $V(N[Ad]Ar)_3$ complex.[25] Ligand binding to **1** will involve displacement of this sort of η^3-allylic interaction, which will influence both the thermodynamics (enthalpy of reaction) and kinetics (enthalpy of activation). The process can in principle occur either through associative displacement of this interaction by the incoming base or by an intramolecular dissociative mechanism in which a vacant site is generated. However, DFT calculations confirm that the corresponding conformer without this interaction is not a minimum in the potential energy surface, indicating that the ligand most likely associatively attacks **1** to essentially dislodge the allylic interaction. Removal of this interaction in **1** by constrained optimizations accounts for about 4 kcal mol^{-1} in the thermochemistry of ligand binding, and likely in the enthalpy of activation as well.

3.1.2. X-ray Structure of 1≡O. The X-ray structure of the diamagnetic tetrahedral complex **1**≡O is shown in Figure 2. It resembles previously reported chalcogenide structures of **1**[26] and that of a related oxo complex reported by Gambarotta and co-workers.[25] Space-filling representation of the structure shown in Figure 2b illustrates the limited amount of free space available for access to the O atom of **1**≡O and by inference that a complex **1**−ONX leading to **1**≡O would have considerable steric constraint in the placement of the XN group.

3.1.3. X-ray Structure of dbabhNO (dbabh = 2,3:5,6-Dibenzo-7-azabicyclo[2.2.1]hepta-2,5-diene). The structures of the majority of the OAT reagents studied here (Scheme 1) are well established. However, this work also utilizes the novel OAT reagent dbabhNO,[27] which can be described as N_2O bound to anthracene. The structure of this compound, which has not been reported to date, is shown in Figure 3. It was prepared following literature procedures and a sample was recrystallized by slow evaporation of a methylene chloride/heptane solution.

The N−N−O angle in dbabhNO of 111.3° compares with that in N_2O of 180° and is in keeping with sp^2 hybridization at the central N of the *N*-nitrosoimide. In addition, for dbabhNO the N−N (1.255 Å) and N−O (1.232 Å) bond lengths are significantly longer than for those N_2O: N−N (1.126 Å) and N−O (1.186 Å).[8] The computed structure of dbabhNO (see Supporting Information) is in good agreement with the crystallographic determination.

3.1.4. Structures and Energies of Selected 1−ONX Adducts. In order to clear up the nature of OAT in the systems studied, the structures of selected **1**−ONX adducts were also computed. Since **1** has two unpaired electrons and **1**≡O is diamagnetic, it is clear that an intersystem crossing between the triplet and singlet potential energy surfaces must occur along the path of the reaction. This process can in principle happen either before or after adduct formation. Therefore, the structures of adducts for both the singlet and triplet states were calculated. Computational results on structures and energies of the adducts are summarized in Table 1.

For the N_2O (O-bound), PyO, and MesCNO adducts, minima were only found in the triplet potential energy surface. For the rest, different minima were obtained for both the singlet and triplet states. The trigonal planar nature of **1** is not greatly altered upon formation of the high-spin adducts in the N_2O (O-bound) and PyO adducts. The degree of pyramidalization of the VN_3 moiety can be quantified by the sum of the three N−V−N bond angles being about 353° in the adducts as compared with ∑(N−V−N) = 356.1° in **1**. While binding of PyO results in little deviation from planarity and the complex has a relatively long V−O bond length (2.007 Å), the situation is quite different for binding of PhNO in both triplet and singlet states (and also for the IMe/N_2O and SIMe/PhCNO adducts). For singlet **1**−ONPh, the V−O bond of 1.751 Å is contracted significantly, being closer to that found in **1**≡O (1.590 Å), and the ∑(N−V−N) of 336.9° also compares to that for **1**≡O of 336.7°. The structure of triplet **1**−ONPh resembles that of the singlet, and there is little change in ∑(N−V−N) for the two complexes. It should be noted that the triplet form in the case of PhNO, MesCNO, IMe/N_2O, and SIMe/PhCNO is different in character from that of the complexes of N_2O (O-bound) and PyO. While DFT-calculated Mulliken spin densities for the vanadium center are essentially 2 for the latter complexes,

dx.doi.org/10.1021/ja405395z | J. Am. Chem. Soc. 2013, 135, 11357−11372

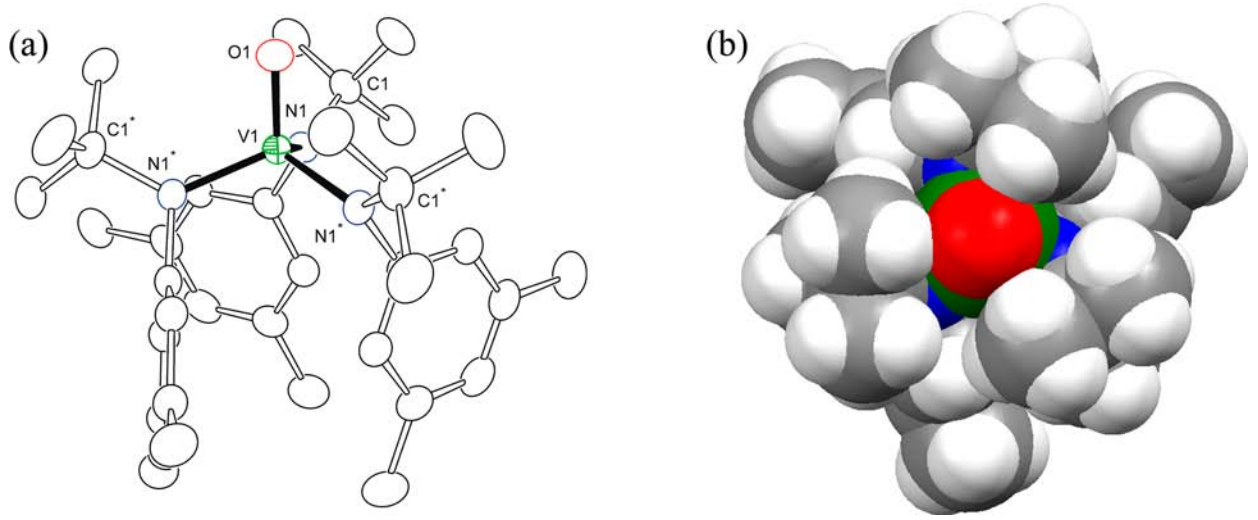

Figure 2. (a) Drawing of **1**≡O with thermal ellipsoids at the 30% probability level. Selected interatomic distances (Å) and angles (deg): V1−O1 = 1.590(3); V1−N1 = 1.883(2); O1−V1−N1 = 107.87(5); N1−V1−N1* = 111.03(5). (b) Space filling model showing access to O (red) bonded to V (green); N (blue), C (gray), and H (white) are also shown.

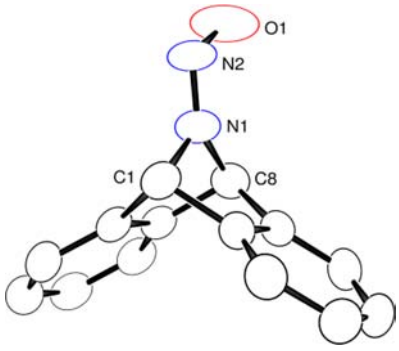

Figure 3. Drawing of dbabhNO with thermal ellipsoids at the 40% probability level. Selected interatomic distances (Å) and angles (deg): C1−N1 = 1.468(3); C8−N1 = 1.492(3); N1−N2 = 1.255(7); N2−O1 = 1.232(8); N2−N1−C1 = 119.7(4); N2−N1−C8 =141.1(4); C1−N1−C8 = 99.2(2); O1−N2−N1 = 111.3(8).

Mulliken spin densities ranging from 1.20 to 1.50 were obtained for the triplet adducts of PhNO, MesCNO, IMe/N_2O, and SIMe/PhCNO, supporting substantial electron transfer from the metal to the ligand in these adducts.

When both singlet and triplet minima were found for a certain adduct, the singlet state was generally lower in energy in keeping with a stronger interaction between the metal fragment and the ligand. However, in the case of the SIMe/PhCNO adduct of **1**, this pattern is reversed. This behavior can be easily understood in terms of the alleviation of the steric strain imposed by this bulky ligand in the triplet as compared with the singlet state since the V−O bond length is longer in the high-spin structure. Moreover, calculations were performed for a truncated model where the 2,6-diisopropylphenyl substituents on the nitrogen atoms of the NHC in the real system were replaced by methyl groups and the mesityl group by a phenyl ring. In the real system, SIPr/MesCNO, the energetic difference favoring the high-spin over the low-spin structure is expected to be even higher. For the IMe/N_2O truncated model of IPr/N_2O, DFT calculations predict a very small energetic difference between the singlet and triplet adducts. Thus, it is conceivable that both species can coexist in equilibrium once the adduct is formed.

A number of η^2 complexes of PhNO are known, and the structure of the minimum energy η^2 singlet structure was computed. This species is 2.8 kcal mol^{-1} higher in energy than

Table 1. Computational Summary of Binding to 1[a]

ligand	multiplicity	V−O (Å)	V−O−N (deg)	∑(N−V−N)[e] (deg)	ΔH_{bind}[a] (kcal mol^{-1})
N_2O	triplet	2.164	140.6	352.7	12.1
N_2O[b]	triplet	1.856[c]	168.1[d]	343.3	3.1
N_2O[b]	singlet	1.710[c]	170.5[d]	335.9	−7.1
PyO	triplet	2.007	134.0	353.7	−2.3
MesCNO	triplet	1.849	122.6	339.3	4.1
IMe/N_2O[f]	triplet	1.869	131.4	342.6	−18.6
IMe/N_2O[f]	singlet	1.756	156.9	340.1	−18.3
SIMe/PhCNO[f,g]	triplet	1.874	126.8	338.9	−11.8
SIMe/PhCNO[f,g]	singlet	1.796	137.8	336.3	−7.7
PhNO	triplet	1.888	123.9	338.7	−24.1
PhNO	singlet	1.751	142.3	336.9	−31.3

[a]Calculated at the bp86/6-311G(d,p) (MDF10 for V with an additional set of f functions) level. [b]N-bound adduct. [c]V−N bond length. [d]V−N−N angle. [e]Sum of the three $(N-V-N)_{anilides}$ bond angles. [f]calculations corresponding to the adduct with a truncated model where the 2,6-diisopropylphenyl substituents of the nitrogens of the N-heterocyclic carbene in the real system have been replaced by methyls. [g]Calculations corresponding to the adduct with a truncated model where the mesityl group has been replaced by a phenyl ring.

dx.doi.org/10.1021/ja405395z | J. Am. Chem. Soc. 2013, 135, 11357−11372

the corresponding η^1 singlet adduct, presumably due to steric factors in the bulky trisanilide complex **1**. Likewise, minimum energy η^2-adducts were found computationally for the **1**−ON_2/IMe and **1**−ONCPh/SIMe complexes being 7.0 and 15.8 kcal mol^{-1} higher in enthalpy, respectively, than the corresponding most stable η^1-minima in the triplet state. Stable minima corresponding to an η^2 complex were not found for the rest of the XNO reagents studied in the current work.

In binding of N_2O, no stable minimum energy configuration was found for a 1,3-cyclic structure of the adduct of **1**. A minimum energy η^1 (O-bound) triplet state was computed. The computed enthalpy of binding of +12.1 kcal mol^{-1} coupled with an unfavorable entropy of binding means that this complex is inherently unstable. Furthermore, N-bound adducts for both the singlet and triplet states were found with an enthalpy of binding of −7.1 and +3.1 kcal mol^{-1}, respectively. These data are in keeping with marginal thermodynamic stability since an unfavorable entropy of binding will cancel the favorable enthalpic term in the case of the singlet adduct. The bent nature of the NNO ligand in **1**−NNO as well as its singlet ground state is in contrast to the first reported structural determination of an M−NNO complex by Piro and Chang.[8] The (tpa^{Mes})VNNO complex has a triplet ground state and a linear NNO ligand binding architecture. This may be attributed to electronic factors associated with the axial base ligand binding in the (tpa^{Mes})VNNO. It has the consequence that N_2O binds to the (tpa^{Mes})V and the spin state and oxidation number of V remain unchanged in the stable paramagnetic compound (tpa^{Mes})VNNO. The computed structure for **1**−NNO can be viewed as having undergone spin pairing and oxidative addition to form a V(V) complex **1**═N−N═O. This structure is in keeping with the nitrosoimido formulation predicted by previous computational calculations in some related species,[6,7] as well as analogous structurally characterized products.[28]

3.2. Thermochemical Studies. *3.2.1. BDE in 1≡O.* In order to determine the enthalpic changes associated with dissociation of the V−O bond in **1**≡O, calorimetric studies were made in toluene solution for OAT to **1** as shown in eqs 2 and 3. Using values of the N−O BDE in MesCNO

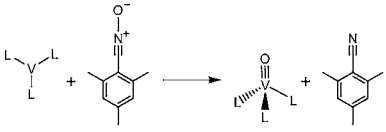

$\Delta H = -102.3 \pm 1.2$ kcal mol^{-1} (2)

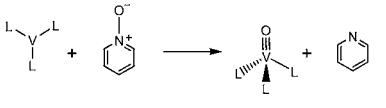

$\Delta H = -90.1 \pm 2.0$ kcal mol^{-1} (3)

(53.1 kcal mol^{-1})[29] and PyO (63.3 kcal mol^{-1})[29] gives estimates of $\Delta H_{V-O,disc}$ of 155.4 and 153.4 based on enthalpies of reactions 2 and 3, respectively. An average value of 154 ± 3 kcal mol^{-1} is adopted for this value in toluene solution (Table 2). The value obtained from DFT calculations of 151.3 kcal mol^{-1} is in good agreement with the experimental value.

3.2.2. N−O BDE in dbabhNO. In order to determine the N−O BDE of dbabhNO, the enthalpy of reaction 4

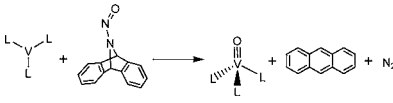

$\Delta H = -142.6 \pm 1.9$ kcal mol^{-1} (4)

Table 2. Experimental and Computational X−O BDE for Selected Species

bond	compound	BDE_{calc}[a] (kcal mol^{-1})	BDE_{expt} (kcal mol^{-1})
N−O	dbabhNO	10.4[b]	9.7 ± 3.0[b]
N−O	IPr/N_2O	62.0	
N−O	SIPr/MesCNO	74.6	
N−O	PhNO	108.2	
V−O	**1**≡O	151.3	154 ± 3

[a]Calculated at the bp86/6-311G(d,p) level (MDF10 with an additional set of f functions for V). [b]This BDE value includes rearrangement of the unstable dbabhN fragment to anthracene and N_2.

was measured. Utilizing the V−O BDE of 154 ± 3 kcal mol^{-1} in **1**≡O and data in eq 4 yields an N−O BDE of 11.4 ± 4.9 kcal mol^{-1} for dbabhNO. As a check on this value, the thermal decomposition shown in eq 5 was investigated by differential

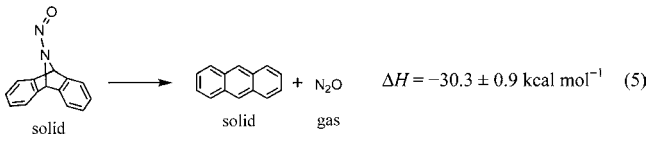

$\Delta H = -30.3 \pm 0.9$ kcal mol^{-1} (5)

scanning calorimetry between 30 and 150 °C. Utilizing the enthalpy of formation of anthracene (28.9 ± 2.4 kcal mol^{-1})[30] and N_2O (19.6 kcal mol^{-1})[30] yields an absolute enthalpy of formation of dbabhNO (s) of 78.8 ± 3.3 kcal mol^{-1}. The enthalpy of dissociation of N_2O (eq 6)[30] is known.

$$N_2O(g) \rightarrow N_2(g) + O(g) \quad \Delta H = 39.5 \text{ kcal mol}^{-1} \qquad (6)$$

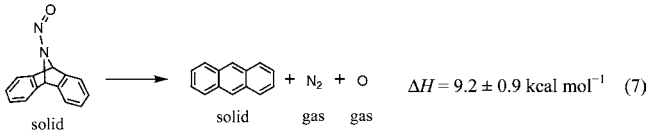

$\Delta H = 9.2 \pm 0.9$ kcal mol^{-1} (7)

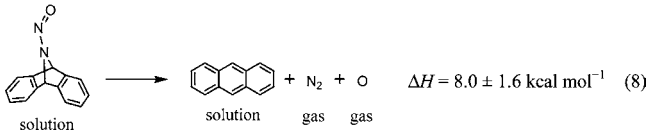

$\Delta H = 8.0 \pm 1.6$ kcal mol^{-1} (8)

Addition of eqs 5 and 6 yields eq 7. Correction of the solid phase reaction in eq 7 to that in solution as shown in eq 8 was made by measurement of the enthalpies of solution of dbabhNO (s) (3.8 ± 0.4 kcal mol^{-1}) and anthracene (s) (5.0 ± 0.2 kcal mol^{-1}) in toluene and utilizing Hess's law. The value of the N−O BDE in toluene solution of dbabhNO is 11.4 ± 4.9 kcal mol^{-1} based on eq 4 and 8.0 ± 1.6 kcal mol^{-1} based on eq 8. We adopt the average value 9.7 ± 3.0 kcal mol^{-1}. This is in perfect agreement with the value obtained from DFT calculations of 10.4 kcal mol^{-1} (Table 2). This BDE value includes rearrangement of the unstable dbabhN fragment formed on cleaving the N−O bond to anthracene and N_2, which are the observed reaction products. Reaction 8 should have an entropy of reaction positive enough to make it thermodynamically favorable at room temperature.[31] The authors are not aware of other stable crystalline compounds that can provide a free ^{3}O atom with a negative Gibbs energy of reaction. Additional synthetic and thermochemical studies of the reactivity of dbabhNO are in progress.

dx.doi.org/10.1021/ja405395z | J. Am. Chem. Soc. 2013, 135, 11357−11372

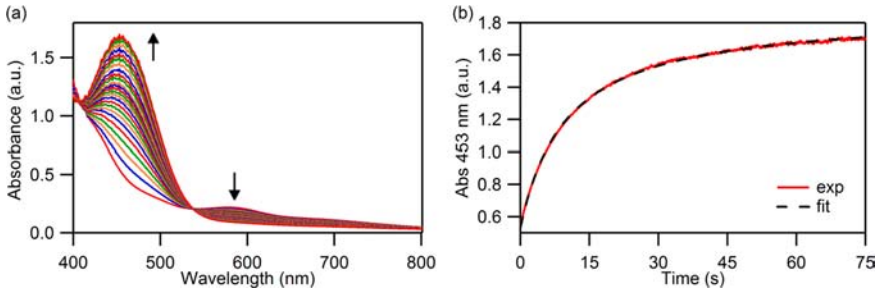

Figure 4. (a) Time-resolved spectra obtained from the reaction between **1** (0.3 mM) and N_2O (66 mM) in toluene over 75 s at 25 °C. (b) Kinetic trace at λ = 453 nm (red) with second-order fit (black dashed line).

3.2.3. Calorimetric Measurement of the Enthalpy of Binding of PhNO to 1. The enthalpy of binding of PhNO to **1** was estimated using Calvet calorimetry at 30 °C in toluene solution and resolving the thermogram into a rapid first step (binding) and a slower secondary step (actual OAT). The derived value of approximately −45 kcal mol^{-1} at 30 °C, though approximate in nature, was higher than the DFT-computed enthalpy of binding of −31.3 kcal mol^{-1} (Table 1) and prompted investigation by isoperibol calorimetry at 5 °C in toluene. Ampoules of approximately 5 mL volume containing the blue solution of fully dissociated PhNO were broken into 350 mL of toluene solution containing a large excess of **1**, and the enthalpy of reaction generated in the first ∼100 s of reaction were measured. Under these conditions, NMR studies show that OAT occurs to a negligible amount, and any small heat generated would be absorbed into the final baseline of the thermogram. The value of ΔH = −54 ± 2 kcal mol^{-1} is the average of three separate determinations based on use of sublimed PhNO as limiting reagent.

3.3. Kinetic Studies. The kinetics of the OAT reactions were studied by the stopped flow method, and in all cases time-resolved UV−visible spectra showed conversion of **1** to **1**≡O (λ_{max} = 453 nm) in toluene. For PhNO, variable-temperature NMR experiments were necessary to study the kinetics of **1**≡O formation. Four categories of kinetic behavior were observed and are discussed in the following order: (I) dinuclear OAT following an overall third-order rate law (N_2O); (II) formation of stable oxidant-bound complexes followed by OAT in a separate step (PyO and PhNO); (III) transient formation and decay of metastable oxidant-bound intermediates on the time scale of OAT (SIPr/MesCNO and IPr/N_2O); (IV) steady-state kinetics in which no detectable intermediates are observed (dbabhNO and MesCNO).

3.3.1. Category I: Dinuclear OAT Following a Third-Order Rate Law (N_2O). OAT from N_2O to **1** occurs within minutes at room temperature. Time-resolved spectra acquired over a broad temperature range (−62 to 25 °C) showed clean conversion with no detectable intermediates (Figure 4a). Kinetic traces obtained at the three highest temperatures (7, 16, and 25 °C) under pseudo-first-order conditions (excess N_2O) did not fit to a rate law that is first order in concentration of **1**; instead, as shown in Figure 4b, excellent fits were obtained from a rate law that is second order in concentration of **1** and first order in concentration of N_2O, yielding an overall third-order rate law.

Derived third-order rate constants of 4670 ± 285 M^{-2} s^{-1} (25 °C), 5380 ± 512 M^{-2} s^{-1} (16 °C), and 6870 ± 136 M^{-2} s^{-1} (7 °C) were obtained from the slopes of the linear plots of the observed second-order rate constant (k_{eff}) versus N_2O concentration as shown in Figure S8, Supporting Information. Activation parameters for the high temperature third-order reaction were $\Delta H^{\ddagger}_{3rd\text{-}order}$ = −4.1 ± 0.5 kcal mol^{-1} and $\Delta S^{\ddagger}_{3rd\text{-}order}$ = −56 ± 2 cal mol^{-1} K^{-1}. The large negative activation entropy is in keeping with a ternary transition state, while the negative composite activation enthalpy suggests an exothermic binding of N_2O to **1** followed by formation of a transition state **1**−ONN−**1** with a low barrier to oxidative addition.

At −14 °C, the kinetic traces could not be fit well to either first- or second-order rate laws with respect to concentration of **1**. As discussed later, the behavior at intermediate temperature could be successfully modeled in terms of an overall mechanism of mixed reaction order, but temperature resolution into two limiting regimes, overall third-order (second-order in **1**) at high T and overall second-order (first-order in **1**) at low T, provided the initial convincing evidence for the mechanism. At low temperatures (−62, −53, −35 °C), the reaction was found to obey a rate law first order in concentration of **1** and in concentration of N_2O. Spectra and analysis are provided in Supporting Information, and the derived overall second-order rate constants (k_1) were 0.055 ± 0.005 M^{-1} s^{-1} (−62 °C), 0.119 ± 0.006 M^{-1} s^{-1} (−53 °C), and 0.386 ± 0.007 M^{-1} s^{-1} (−35 °C). Activation parameters for the low temperature second-order reaction were $\Delta H^{\ddagger}$ = 6.7 ± 0.3 kcal mol^{-1} and $\Delta S^{\ddagger}$ = −32 ± 1 cal mol^{-1} K^{-1}.

The change in reaction order and in the sign of effective activation enthalpy as a function of temperature also suggests stepwise bimetallic activation of N_2O in which the rate-determining step changes with temperature. Dinuclear activation of N_2O by the mechanism shown in eq 9 and

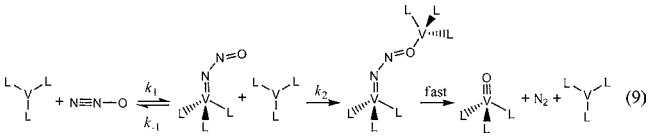

(9)

assuming a steady state in concentration of **1**−NNO (in keeping with the clean isosbestic points and failure to detect a spectroscopically observable intermediate) yields the rate law shown in eq 10.

$$\text{rate} = \frac{k_1 k_2 [\mathbf{1}]^2 [N_2O]}{(k_{-1} + k_2[\mathbf{1}])} \quad (10)$$

This will yield two limiting rate laws: if $k_{-1} \gg k_2[\mathbf{1}]$, overall third-order kinetics will be observed with $k_{obs} = (k_1 k_2 / k_{-1})$. On the other hand, if $k_2[\mathbf{1}] \gg k_{-1}$, second-order kinetics will be followed with $k_{obs} = k_1$.

The observed kinetic behavior over the entire temperature range is consistent with this type of mechanism. This was

dx.doi.org/10.1021/ja405395z | J. Am. Chem. Soc. 2013, 135, 11357−11372

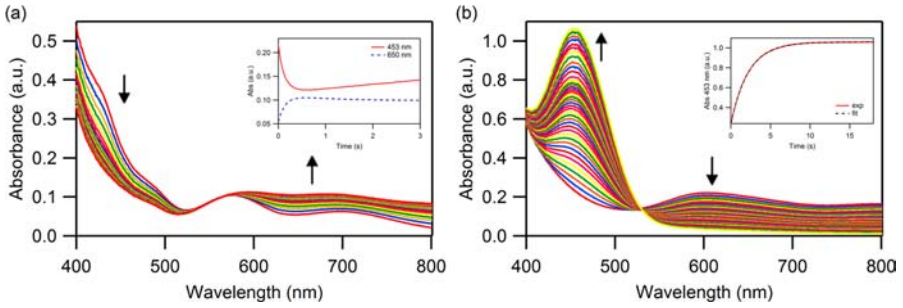

Figure 5. (a) Diode array spectral changes accompanying the reaction between **1** (0.3 mM) and PyO (2 mM) at −80 °C acquired over 580 ms, showing growth of **1**−OPy (longer wavelengths) with decay of **1** at shorter wavelengths and an isosbestic point near 570 nm. Inset shows kinetic traces at λ = 453 and 650 nm. Longer reaction times show slow conversion to **1**≡O. (b) Diode array spectral changes accompanying the reaction between **1** (0.2 mM) and PyO (10 mM) at 0 °C acquired over 18 s, showing formation of **1**≡O (λ = 453 nm) with concomitant decay of rapidly formed **1**−OPy occurring at longer wavelengths. Inset shows kinetic trace at λ = 453 nm with single exponential fit.

followed by full computer simulation of the data over all temperatures to the rate law in eq 10, which was in excellent agreement with the experimental data (see Supporting Information). The activation parameters derived from the kinetic model are $\Delta H_1^{\ddagger}$ = 6.3 ± 0.3 kcal mol^{-1} and $\Delta S_1^{\ddagger}$ = −34 ± 1 cal mol^{-1} K^{-1} for k_1; $\Delta H_{-1}^{\ddagger}$ = 13 ± 1 kcal mol^{-1} and $\Delta S_{-1}^{\ddagger}$ = −6 ± 1 cal mol^{-1} K^{-1} for k_{-1}; and $\Delta H_2^{\ddagger}$ = 3.0 ± 0.1 kcal mol^{-1} and $\Delta S_2^{\ddagger}$ = −27 ± 1 cal mol^{-1} K^{-1} for k_2. The predicted third-order activation parameters of $\Delta H_{\text{3rd-order}}^{\ddagger}$ = $\Delta H_{(k_1+k_2-k_{-1})}^{\ddagger}$ = (6.3 + 3.0 − 13) = −3.7 kcal mol^{-1} and $\Delta S_{\text{3rd-order}}^{\ddagger}$ = $\Delta S_{(k_1+k_2-k_{-1})}^{\ddagger}$ = (−34 + (−27) − (−6)) = −55 cal mol^{-1} K^{-1} are in excellent agreement with the direct experimental estimates from the high-temperature data discussed above. The crossover in reaction mechanism is due to the high activation energy for the dissociation step (k_{-1}) causing it to overtake k_2 at higher T. The enthalpy of binding of N_2O, ΔH^0 = ($\Delta H_{k_1}^{\ddagger}$ − $\Delta H_{k_{-1}}^{\ddagger}$) = (6.3 − 13) = −6.7 kcal mol^{-1}, is in agreement with the computed enthalpy of binding of N_2O (N-bound, singlet) of −7.1 kcal mol^{-1} (Table 1). The high-temperature third-order reaction has an apparent negative enthalpy of activation and appears to speed up with decreasing temperature. If this reaction were an elementary third-order step rather than a composite one, the change to second-order kinetics and concomitant slowing with temperature would not be observed. Provided k_{-1} has a higher enthalpy of activation than does k_2, the rate will decrease more rapidly with decreasing temperature and cause the observed change in the rate-limiting step. This observed behavior is predicted from the analysis of time-resolved spectral data, supporting the proposed stepwise bimetallic mechanism (eq 9).

3.3.2. Category II: Formation of a Stable Adduct Followed by OAT (PyO and PhNO). The reaction between excess PyO and **1** could be readily separated into ligand binding at low temperatures (−80 to −53 °C) and OAT from **1**−OPy at high temperatures (0−20 °C). Low-temperature time-resolved spectral changes are shown in Figure 5a. A rapid increase in the absorption bands at longer wavelengths was observed, with concomitant decay occurring under ∼550 nm. The observed rate constants obtained from fitting kinetic traces to a single-exponential function depended linearly on PyO concentration, and the second-order rate constants (k_1) representing formation of a **1**−OPy adduct were obtained from the slopes of these plots as shown in Figure S13, Supporting Information. The near zero y-intercepts suggest that this process can be regarded as essentially irreversible over the temperature range studied. An Eyring plot was used to obtain activation parameters for this binding process: $\Delta H_1^{\ddagger}$ = 6.8 ± 0.4 kcal mol^{-1} and $\Delta S_1^{\ddagger}$ = −7 ± 2 cal mol^{-1} K^{-1}. Notable is the low entropy of activation for ligand binding in this system. This may be attributed to concomitant cleavage of the aryl contact in **1** (Figure 1) with a favorable entropic component due to more degrees of freedom in the open form.

At higher temperatures, binding of PyO is too rapid to be observed by the standard stopped flow method, and conversion to the bound **1**−OPy complex occurs rapidly on mixing. This allows for convenient following of the second step in the OAT reaction sequence as the intermediate complex **1**−OPy converts to **1**≡O and Py. Time-resolved spectral data are shown in Figure 5b. The broad, lower energy absorbance band assigned to **1**−OPy (600−800 nm) decays steadily as **1**≡O (λ_{max} = 453 nm) grows in. The observed rate constants measured at high temperatures showed essentially no dependence on PyO concentration (Figure S14, Supporting Information). The reaction was thus treated as zero order in PyO and the average value of k_{obs} was taken as the true first-order rate constant (k_2) for product formation from **1**−OPy. Activation parameters associated with k_2 were derived from an Eyring plot: $\Delta H_2^{\ddagger}$ = 15 ± 1 kcal mol^{-1} and $\Delta S_2^{\ddagger}$ = −4 ± 2 cal mol^{-1} K^{-1}. The OAT reaction shows a high value of $\Delta H^{\ddagger}$ and a negative $\Delta S^{\ddagger}$ that is small in absolute value.

The kinetics of PhNO binding was also studied by the stopped flow method at low temperatures (−80 to −53 °C). The corresponding time-resolved spectral changes revealed rapid formation of intense absorbance bands at λ_{max} = 477 and 740 nm that are assigned to the **1**−ONPh adduct (Figure 6). The rates of formation of the **1**−ONPh adduct were quantified by following the growth in absorbance at λ = 740 nm under pseudo-first-order conditions; observed rate constants depended linearly on PhNO concentration, and y-intercepts were very close to zero (Figure S15, Supporting Information). Activation parameters for PhNO binding were derived from an Eyring plot: $\Delta H_1^{\ddagger}$ = 5.7 ± 0.5 kcal mol^{-1} and $\Delta S_1^{\ddagger}$ = −14 ± 3 cal mol^{-1} K^{-1}.

The rather dramatic changes in spectra upon binding of PhNO to **1** are in contrast to those described earlier for the binding of PyO (Figure 5a). In order to provide additional information on the nature of these adducts observed at low temperature by stopped flow spectrophotometry, ^{1}H NMR studies of ligand binding to **1** at −70 °C were performed for both PhNO and PyO. As shown in Supporting Information, PhNO yielded a diamagnetic complex with narrow peaks in its ^{1}H NMR spectrum. In contrast, PyO was confirmed to form a paramagnetic complex upon mixing at −70 °C, and very slow OAT to form Py and **1**≡O was observed at this temperature.

dx.doi.org/10.1021/ja405395z | J. Am. Chem. Soc. 2013, 135, 11357−11372

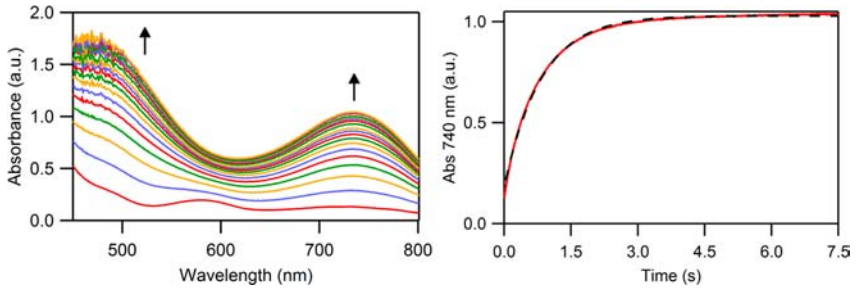

Figure 6. (left) Diode array spectral changes upon reaction of **1** (0.3 mM) with excess PhNO (1 mM) at −80 °C over 7.5 s. (right) Kinetic trace at λ = 740 nm (red) with single exponential fit (black dashed line).

Therefore, the differences in UV−vis spectra observed between **1**−OPy and **1**−ONPh can be explained by the different spin states of vanadium (high-spin versus low-spin) in these adducts as determined by NMR studies and in keeping with DFT calculations described earlier. Furthermore, TD DFT calculated UV−vis spectra for both species are in keeping with the experimental spectral changes.

Over a 1 h time period, **1**≡O formation from **1**−ONPh was not observed to occur to a measurable extent at −70 °C. However, the room temperature ^{1}H NMR spectrum of PhNO and **1** show clear formation of **1**−ONPh, which slowly converts to **1**≡O and other products. As shown in Figure S3, Supporting Information, the NMR signals due to **1**−ONPh and **1**≡O were suitable for kinetic analysis. Rate constants for the formation of **1**≡O from **1**−ONPh were 0.00031 ± 0.00006 s^{-1} (22 °C), 0.0015 ± 0.0003 s^{-1} (35 °C), and 0.0034 ± 0.0007 s^{-1} (45 °C). Derived activation parameters (Figure S5, Supporting Information) are $\Delta H_2^{\ddagger}$ = 19 ± 2 kcal mol^{-1} and $\Delta S_2^{\ddagger}$ = −9 ± 5 cal mol^{-1} K^{-1}.

In the absence of added reagents, the reaction occurs according to eq 11. Decomposition of *in situ* **1**−ONPh to **1**≡O

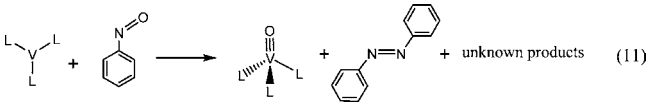

(11)

is nearly quantitative in terms of V containing products, and the unknown organic products likely result from decomposition of phenyl nitrene, which may be generated either as a free or loosely bound species during the reaction. The yield of PhNNPh was ∼30% of the anticipated PhNNPh based on reaction stoichiometry (eq 11). The unknown products include a dark precipitate and an unknown paramagnetic compound with broad peaks in the region of 6−8 ppm. The most likely mechanism is direct expulsion of a nitrene as shown in eqs 12 and 13.

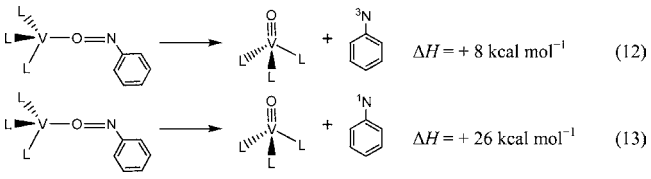

(12)

(13)

Based on the measured enthalpy of binding of PhNO (−54 kcal mol^{-1}), the calculated N−O BDE in PhNO (108.2 kcal mol^{-1}, see Table 2) and a gap of 18 kcal mol^{-1} between the triplet and singlet nitrene,[32] the energetics of nitrene expulsion is readily calculated. As shown in eq 13, the value of +26 kcal mol^{-1} exceeds the observed activation energy of +19 kcal mol^{-1}, and so expulsion of ^{1}NPh can be ruled out not only based on production of PhNNPh[33] but also in terms of energetics. Additional evidence in keeping with expulsion of a free triplet nitrene is generated by the observation that in the presence of excess free PhNO, a well-known trapping species for triplet nitrenes,[34] azoxybenzene is formed, and in the presence of excess **1**, **1**═NPh is also formed. However, more complex mechanisms in which a free nitrene is not generated can also be imagined,[35] and only direct spectroscopic detection of the triplet nitrene can prove its generation. That is beyond the scope of this investigation.

3.3.3. Category III: Transient Formation and Decay of a Metastable Intermediate on the Time Scale of OAT (IPr/N_2O and SIPr/MesCNO). Stopped flow kinetic measurements of the reaction between excess IPr/N_2O (2−12 equiv) and **1** (0.25 mM) were performed over a broad temperature range (−62 to −35 °C). As shown in Figure 7, time-resolved spectral changes showed a rapid, intense growth in absorbance across the entire spectral window with a band centered near λ = 475 nm. A slower decay process follows where the intense band at 475 nm is found to blue shift to the expected maximum for **1**≡O (λ = 453 nm).

For technical reasons, the kinetic data were analyzed at λ = 725 nm, and traces were fit to the general two term rate law, rate = $A_1 \exp(-k_{1,obs}t) + A_2 \exp(-k_{2,obs}t)$.[36] Plots of $k_{1,obs}$ versus IPr/N_2O concentration were linear with nonzero *y*-intercepts, while plots of $k_{2,obs}$ versus IPr/N_2O concentration appeared to saturate. Full analysis of the experimental data is provided in Supporting Information. The results obtained from analysis of the experimental data were verified by global modeling as described in Supporting Information. The proposed mechanism of OAT from IPr/N_2O to **1** occurs through the initial reversible formation of an intensely absorbing intermediate adduct (k_1, k_{-1}), which subsequently decays in the OAT step (k_2), forming **1**≡O. Spectra computed by the kinetics program for the species involved were consistent over the temperature and concentration ranges studied and are shown in Figure 8. The modeled spectrum of **1**−ON_2/IPr is in good agreement with that obtained computationally by TD DFT calculations for the singlet adduct of the truncated model IMe/N_2O (see Supporting Information). Derived activation parameters from the kinetic model were in good agreement with experimentally determined values and are $\Delta H_1^{\ddagger}$ = 5.6 ± 0.4 kcal mol^{-1} and $\Delta S_1^{\ddagger}$ = −18 ± 2 cal mol^{-1} K^{-1} (for ligand binding, k_1) and $\Delta H_2^{\ddagger}$ = 13 ± 1 kcal mol^{-1} and $\Delta S_2^{\ddagger}$ = 1 ± 2 cal mol^{-1} K^{-1} (for OAT, k_2).

Analogous to the reactions with IPr/N_2O, the time-resolved spectral changes accompanying the reaction between excess

dx.doi.org/10.1021/ja405395z | J. Am. Chem. Soc. 2013, 135, 11357−11372

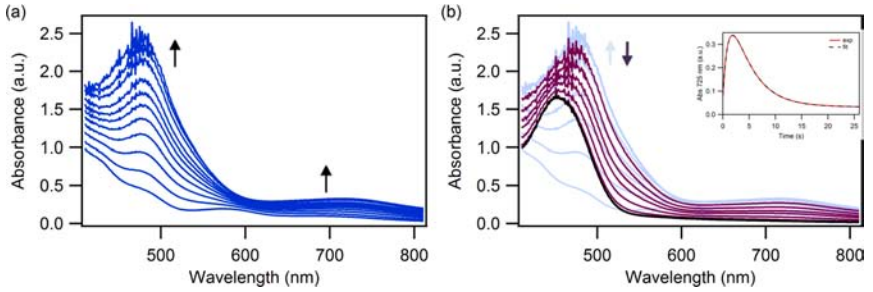

Figure 7. Time-resolved spectra obtained from the reaction of **1** (0.25 mM) with IPr/N_2O (1 mM) at −62 °C acquired over 26 s. (a) Rapid formation of the intermediate is observed initially across the entire spectral window, which maximizes within ca. 2 s. (b) Decay of the intensely absorbing intermediate (purple traces) superimposed on its prior accumulation, ultimately ending with the expected spectrum of **1**≡O (black trace). Inset shows the kinetic trace at λ = 725 nm with double-exponential fit.

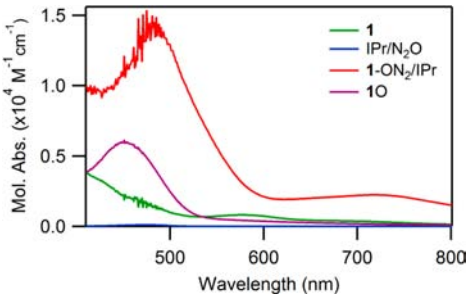

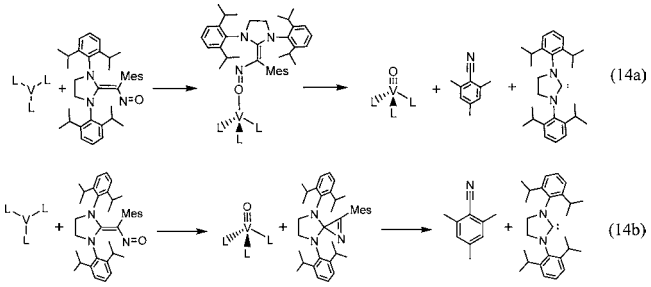

Figure 8. Spectra computed of colored components by the kinetics program, obtained from modeling at −62 °C with $[\mathbf{1}]_o$ = 0.25 mM and $[IPr/N_2O]_o$ = 2 mM. A known spectrum of IPr/N_2O was used while all other species were calculated. The computed spectra of **1** and **1**≡O are in good agreement with their actual spectra.

SIPr/MesCNO (2−12.5 equiv) and **1** (0.3 mM) at low temperatures (−80 to −62 °C) could be divided into two parts as shown in Figure 9. The first stage of the reaction is also characterized by a rapid, intense growth in absorbance over the entire spectral region (Figure 9a). In the second stage, there is a leveling off in the absorbance near that seen for **1**≡O at 453 nm, but at wavelengths above 500 nm, there is steady decrease in absorption (Figure 9b, inset). At higher temperatures, however, the intensely absorbing species was not detected, and only clean, rapid conversion of **1** to **1**≡O was observed with isosbestic points near λ = 415 and 525 nm.

Two possible sources of the colored intermediate were considered as shown in eqs 14a and 14b. The accepted mechanism that best fits the kinetic data and calculated spectroscopic data is one in which the colored intermediate is due to the adduct formed between **1** and MesCNO/SIPr as shown in eq 14a. An alternative mechanism considered is shown in eq 14b, in which the colored intermediate is due to a metastable organic intermediate, the deoxygenated adduct SIPr/MesCN.

A stable azirine formed by reaction of an NHC with a nitrile has been reported recently[37] though it was found to be pale yellow. TD DFT calculations predict a low intensity band at λ = 473 nm for the SIPr/MesCN fragment (See Supporting Information), but the absorption observed at longer wavelengths due to the intermediate formed in stopped flow experiments cannot be attributed to this fragment. However, the TD DFT computed spectrum of the triplet **1**−ONCPh/SIMe truncated model for the adduct (See Supporting Information) is in keeping with kinetic modeling studies in which the spectral changes in Figure 9 are in fact due to complex formation and decay in a manner similar to that described for IPr/N_2O above. Full analysis of the experimental data and details of kinetic modeling are provided in the Supporting Information. Derived activation parameters are $\Delta H_1^{\ddagger}$ = 4.9 ± 0.4 kcal mol^{-1}, $\Delta S_1^{\ddagger}$ = −19 ± 2 cal mol^{-1} K^{-1}

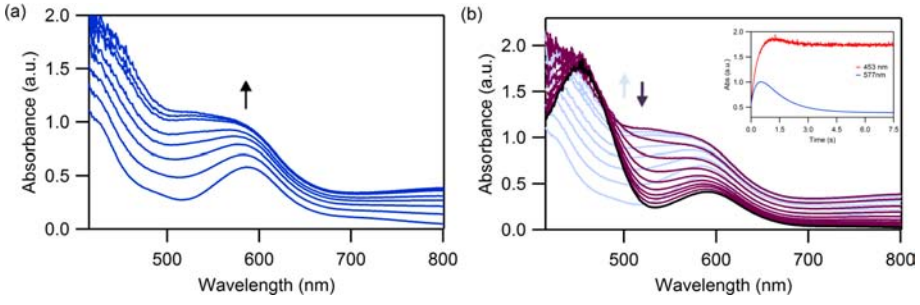

Figure 9. Time-resolved spectra obtained from the reaction of **1** (0.3 mM) with SIPr/MesCNO (3 mM) at −80 °C acquired over 7.5 s. (a) Initial stage of the reaction (0−0.6 s) where rapid adduct formation is observed. (b) Spectral changes during the second phase of the reaction (0.6−7.5 s) showing decay of the broad lower energy bands (purple traces) superimposed on its prior accumulation. Inset shows kinetic traces at λ = 453 and 577 nm.

dx.doi.org/10.1021/ja405395z | J. Am. Chem. Soc. 2013, 135, 11357−11372

(for ligand binding, k_1) and $\Delta H_2^{\ddagger} = 9.3 \pm 0.3$ kcal mol^{-1}, $\Delta S_2^{\ddagger} = -9 \pm 1$ cal mol^{-1} K^{-1} (for OAT, k_2).

3.3.4. Category IV: Steady-State Kinetics in Which No Detectable Intermediates Are Observed (dbabhNO and MesCNO). The kinetics of the OAT reaction between **1** and dbabhNO were measured at low temperatures (−71 to −44 °C) using excess dbabhNO (3.3−33.3-fold excess). The intense absorbance band at λ = 453 nm corresponding to **1**≡O grew in within seconds as shown in Figure S32, Supporting Information. Absorbance bands assignable to an intermediate dbabhNO−**1** adduct were not detected in the time-resolved spectra; only clean formation of **1**≡O from **1** with isosbestic points near λ = 417 and 526 nm was observed. Kinetic traces fit well to single-exponential rate law, and linear plots of the observed rate constant (k_{obs}) as a function of dbabhNO concentration yielded second-order rate constants (k_{app}), where, assuming a steady state in intermediate adduct, $k_{app} = k_1k_2/(k_{-1} + k_2) = k_1/(1 + k_{-1}/k_2)$ for product formation. Since intermediates were not detected in these reactions, the composite rate constant cannot be broken down further. Activation parameters for the composite reaction were derived from an Eyring plot: $\Delta H^{\ddagger} = 6.3 \pm 0.3$ kcal mol^{-1} and $\Delta S^{\ddagger} = -13 \pm 1$ cal mol^{-1} K^{-1}.

Reactions of excess MesCNO (12−93-fold excess) with **1** (0.3 mM) showed similar spectroscopic behavior to that of dbabhNO as shown in Figure S30, Supporting Information. Unlike dbabhNO, the linear plots of k_{obs} versus MesCNO concentration appeared to give nonzero intercepts, which suggests that k_{-1} plays a role in the kinetic scheme. Derived activation parameters from an Eyring plot were $\Delta H^{\ddagger} = 5.3 \pm 0.8$ kcal mol^{-1} and $\Delta S^{\ddagger} = -24 \pm 3$ cal mol^{-1} K^{-1}. Despite a slightly lower value of $\Delta H^{\ddagger}$ (∼1 kcal mol^{-1}), the rate constant for reaction of MesCNO at −62 °C (81 M^{-1} s^{-1}) is over 20 times smaller than that for dbabhNO at the same temperature (1820 M^{-1} s^{-1}) due to the more unfavorable entropy of activation for OAT.

4. DISCUSSION

This paper describes exploration of factors involved in OAT to complex **1** from the nitrogen oxide substrates shown in Scheme 1. Kinetic, thermodynamic, and computational studies are reported and a relatively complete, albeit complex, picture emerges. Thermochemical studies showed that the V−O bond in **1**≡O (BDE = 154 ± 3 kcal mol^{-1}) is one of the strongest metal oxo bonds to be experimentally determined.[38] Computational studies indicate that in the absence of a stabilizing allylic interaction in **1** (see Figure 1), this would be close to 158 kcal mol^{-1}. Reaction of **1** with XNO is exothermic by 46 (PhNO) to 143 (dbabhNO) kcal mol^{-1} for the compounds shown in Scheme 1, which range from 10−108 kcal mol^{-1} in terms of the BDE of the N−O bond broken.

Because individual rate constants and mechanism vary in these systems, it is useful to view the overall efficacy of the XNO reagents under a common set of conditions as shown in Figure 10.

The net rate of OAT, without regard to detailed mechanism, is in the order PhNO ≪ N_2O < PyO < IPr/N_2O < MesCNO < dbabhNO ≈ SIPr/MesCNO. Derived rate constants and their assignments, as well as activation parameters and N−O BDE data are collected in Table 3.

The range of OAT reagents studied, except for N_2O, which undergoes dinuclear OAT, all follow the general kinetic scheme in eq 1. The reaction of N_2O and **1** can also be viewed as following the same pattern if it is considered not as reaction of **1** with N_2O but as reaction between **1** and the **1**−NNO complex as shown in Scheme 1. From the kinetic point of view, an ideal OAT reagent would have a large value for binding (k_1), a low value for dissociation (k_{-1}), and a huge value for actual OAT (k_2). The ratio k_1/k_{-1} is the K_{eq} for substrate binding, and for a good OAT reagent this will necessarily be high, as will the k_2/k_{-1} ratio.

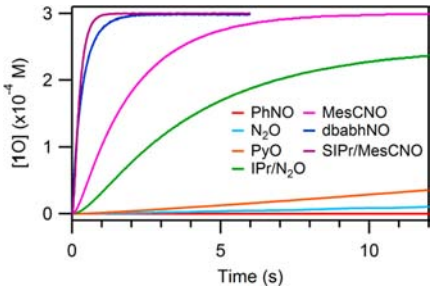

Figure 10. Rate of production of **1**≡O as a function of time at −62 °C under similar conditions. $[XNO]_o$ = 3 mM (SIPr/MesCNO, MesCNO); 2 mM (PyO, PhNO, dbabhNO, IPr/N_2O); 66 mM (N_2O) and $[\mathbf{1}]_o$ = 0.3 mM (for reactions with PhNO, MesCNO, dbabhNO, SIPr/MesCNO, N_2O), 0.25 mM (IPr/N_2O), or 0.2 mM (PyO).

The substrates in Scheme 1 can be divided into linear (MesCNO and N_2O) and bent (PhNO, dbabhNO, IPr/N_2O, SIPr/MesCNO, and **1**═N—N═O) molecules. Only for MesCNO and N_2O can the N bonded to O be viewed as an sp hybrid N atom with true delocalized π-bonding. For PyO, the bonding is primarily dative donation of the basic lone pair of electrons on the Py N atom to O. These and other factors all contribute to influence the rate of OAT in these systems.

It should also be recognized that the act of binding may be quite different for different substrates and this blurs the distinction between simple binding and oxidative addition/OAT. Examples of both high-spin (PyO) and low-spin (PhNO) adduct formation were detected by low T NMR experiments. Thus, the spin crossover event could be considered part of the act of binding or part of the actual OAT itself depending upon the actual potential energy diagram. It is typical to discuss this in terms of the minimum energy crossing point (MECP) as delineated by Harvey.[39] However, it is clear from this work that the crossing point can occur before (PhNO) or after adduct formation (PyO). The computed minimum energy structures of the paramagnetic PyO and diamagnetic PhNO adducts of **1** are shown in Figure 11.

In addition to differing in spin state (S = 1 for **1**−OPy and S = 0 for **1**−ONPh), there is a significant difference in the V−O bond lengths (2.007 vs 1.751 Å) and the degree of pyrimadalization of the V center. The **1**−OPy complex resembles the starting complex **1** in the sense that the three N atoms of the amides are nearly planar, whereas for **1**−ONPh, the adduct is more product like in that it resembles **1**≡O. Furthermore, there is a different arrangement of the N[*t*-Bu]Ar groups; for **1**−ONPh, the *t*-butyl groups are all pointed up toward bound PhNO, and the aryls groups are pointed down and away from it. For **1**−OPy however the computed minimum energy structure has one *t*-butyl group pointing down and two pointing up, probably due to favorable π-stacking interactions between the Py and arene rings of the anilide ligands.[40] These same considerations will play a role in the transition state for binding as well. In the present work, we have not computed the MECPs[39] since that is beyond the scope of our primary experimental goals in the current paper. However, it is clear

Table 3. Data for Reactions of XNO and 1[i]

Category	Substrate	BDE	$k_{assigned}$[a]	k (−62 °C)	$\Delta H^{\ddagger}$	$\Delta S^{\ddagger}$
(I)		40[b]	k_1 (M^{-1} s^{-1})[c]	0.038 ± 0.012	6.3 ± 0.3	−34 ± 1
			k_2 (M^{-1} s^{-1})[c]	very fast[h]	3.0 ± 0.1	−27 ± 1
(II)		63[d]	k_1 (M^{-1} s^{-1})	13,250 ± 540	6.8 ± 0.4	−7 ± 2
			k_2 (s^{-1})	$8.5\cdot10^{-5}$[e]	15 ± 1	−4 ± 2
		108[f]	k_1 (M^{-1} s^{-1})	5,600 ± 79	5.7 ± 0.5	−14 ± 3
			k_2 (s^{-1})	$4.7\cdot10^{-10}$[e]	19 ± 2	−9 ± 5
(III)	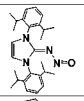	62[f]	k_1 (M^{-1} s^{-1})[c]	785 ± 54	5.6 ± 0.4	−18 ± 2
			k_2 (s^{-1})[c]	0.308 ± 0.014	13 ± 1	1 ± 2
	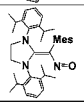	75[f]	k_1 (M^{-1} s^{-1})[c]	3,270 ± 133	4.9 ± 0.4	−19 ± 2
			k_2 (s^{-1})[c]	7.87 ± 0.34	9.3 ± 0.3	−9 ± 1
(IV)		53[d]	$k_{app} = k_1k_2/(k_{-1}+k_2)$ (M^{-1} s^{-1})	81.1 ± 6.2	5.3 ± 0.8	−24 ± 3
		10[g]	$k_{app} = k_1k_2/(k_{-1}+k_2)$ (M^{-1} s^{-1})	1,820 ± 94	6.3 ± 0.3	−13 ± 1

[a]k_1 refers to bimolecular rate constants for XNO binding, k_2 refers to rate constants for OAT, and k_{app} refers to composite bimolecular rate constants for reactions where individual rate constants could not be resolved. [b]Calculated from gas phase data in ref 30. [c]Values taken from kinetic model. [d]Value taken from ref 29. [e]Value extrapolated from Eyring plot for OAT at high T. [f]Calculated at the BP86/6-311G(d,p) level; this value includes dissociation of the deoxygenated adduct to its components in solution. [g]Derived from thermochemical data in this paper and corresponds to the formal reaction **8**. [h]As discussed in Supporting Information, a value of k_2 of 3560 M^{-1} s^{-1} at −62 °C can be determined from modeling studies; however in reality it is the k_2/k_{-1} ratio that is known accurately rather than individual values for k_{-1} and k_2. It can be concluded only that k_2 is very fast even at low T. [i]BDE in kcal mol^{-1}, $k_{assigned}$, k at −62 °C, $\Delta H^{\ddagger}$ in kcal mol^{-1}, and $\Delta S^{\ddagger}$ in cal mol^{-1} K^{-1}.

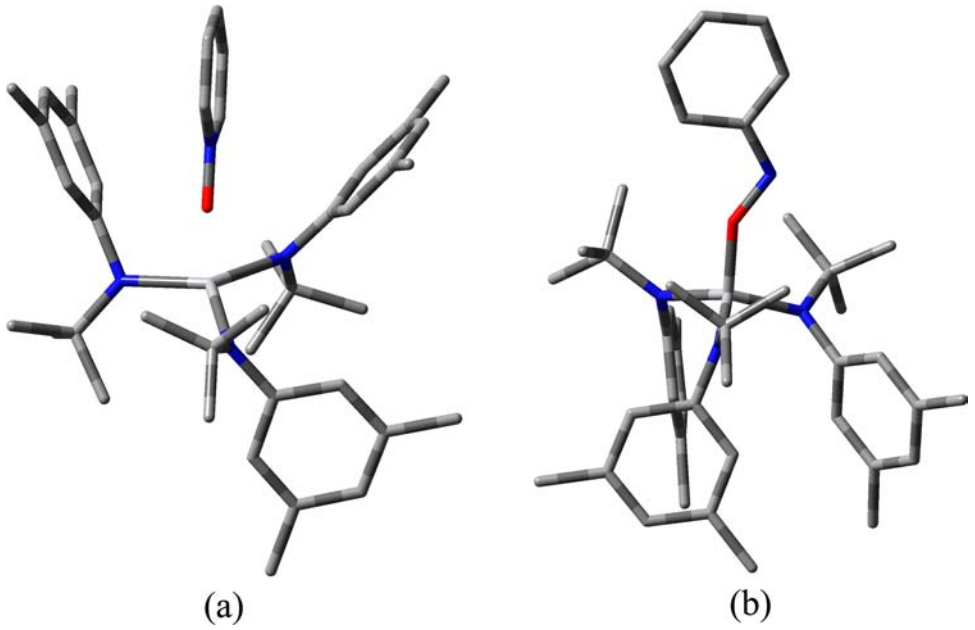

Figure 11. Optimized structure at the bp86/6-311G(d,p) (MDF10 for V with an additional set of f functions) level for (a) **1**−OPy (triplet) and (b) η^1-**1**−ONPh (singlet). For selected interatomic distances and angles, see Table 1.

that the final analysis must include the entire potential energy surface, from binding to spin crossover to expulsion of the reduced OAT reagent, and that spin crossover as well as formal oxidation of V from (III) to (V) may in some cases occur after initial binding and in some cases be part of the binding process itself. A prime example of that is N_2O itself, for which the only computed stable binding mode is through formal oxidation of **1** to produce a computed low-spin V(V) complex, which can be described as being **1**≡N−N═O. In the case where the ligand has low-lying π^* orbitals available to accept electron density from the high-spin complex **1**, the **1**−ONX adduct can be viewed as $\{XNO^{-2\alpha}\}\{\mathbf{1}^{+2\alpha}\}$ (α = 0−1) in which the V(III) has already been oxidized to V(III+2α) where α represents the degree of charge transfer.

Despite these complexities, the enthalpy of activation for binding in all systems where ligand coordination rates were measured (Table 3) is on the order of 6 ± 1 kcal mol^{-1} independently of whether the adduct formed is in low or high

dx.doi.org/10.1021/ja405395z | J. Am. Chem. Soc. 2013, 135, 11357−11372

spin and is not much higher than that estimated for breaking the η^3-arene interaction present in **1** of 4 kcal mol^{-1}. This implies that ligand binding to **1** lacking this interaction should be only on the order of 2 kcal mol^{-1}, in keeping with the generally low activation enthalpy for ligand addition to a metal center with a vacant orbital available for bonding. Since the enthalpies of activation for ligand binding are relatively constant, the entropy of activation plays a strong role in determining the rate constant values. Detailed computational study of oxidant binding in this system is planned, in particular the entropy of activation may be influenced by the nature of the complex formed.

Following brief discussions of rate constant data, each OAT reagent is discussed separately. As mentioned earlier, full computational study of this system is planned and may yield additional insight, and the focus of the current paper is the range of experimental results.

4.1. Rate Constants for Substrate Binding (k_1), OAT (k_2), and Composite Reactions ($k_1k_2/(k_{-1} + k_2)$). For PyO and PhNO, it was possible to measure both the rate of initial binding and the rate of the actual OAT reaction itself and to characterize the intermediate adducts by low T NMR spectroscopy. The intermediate adducts formed between IPr/N_2O or SIPr/MesCNO and **1** were observed to rapidly form and decay in stopped flow experiments. Nevertheless, it proved possible to obtain individual rate constants by kinetic modeling. For MesCNO and dbabhNO, however, no detectable intermediate complexes were observed, and only the composite steady-state rate constants could be determined. This provides some upper and lower limits for estimation of rate constants provided the steady-state assumption is valid. For N_2O, the rate of binding could be resolved by kinetic analysis, but this involves binding through N rather than O. For systems where individual rate constants have been resolved, either directly or through kinetic modeling, a summary of individual rate constants is presented in Table 4 for both binding (k_1) and actual OAT (k_2) at the common temperature of −62 °C.

Table 4. Measured or Modeled Values of Rate Constants at −62 °C

substrate	k_1 (M^{-1} s^{-1})	substrate	k_2 (s^{-1})
PyO	$(13 \pm 1) \times 10^3$	**1**−NNO	very fast[b]
PhNO	$(5.6 \pm 0.1) \times 10^3$	SIPr/MesCNO	7.9 ± 0.3
SIPr/MesCNO	$(3.3 \pm 0.1) \times 10^3$	IPr/N_2O	$(3.1 \pm 0.1) \times 10^{-1}$
IPr/N_2O	$(7.8 \pm 0.5) \times 10^2$	PyO	8.5×10^{-5}[a]
N_2O	$(3.8 \pm 1.2) \times 10^{-2}$	PhNO	4.7×10^{-10}[a]

[a]Value extrapolated from Eyring plot (See Supporting Information). [b]See footnote *h* in Table 3.

The rate of binding is in the order PyO > PhNO > SIPr/MesCNO > IPr/N_2O ≫ N_2O and spans almost 6 orders of magnitude. The rates of actual OAT, where they could be determined, show an even wider range of values (10 orders of magnitude) with the descending order: SIPr/MesCNO > IPr/N_2O ≫ PyO ≫ PhNO. In reactions with N_2O, the proposed intermediate **1**≡N—N═O cannot be detected, but kinetic analysis suggests it to be a rapid OAT reagent to free **1**.

The rate constants for binding of the substrates to **1** at −62 °C in Table 4 can be compared with the recently published value[41] of 2.6×10^4 M^{-1} s^{-1} for O_2 binding to form a low-spin η^1-**1**−O_2 adduct. The very fast rate for O_2, faster even than PyO (Table 4), may be attributed to its small size, as well as the fact that it may approach and bind from either end of the molecule giving it a larger open steric window for binding. Of special note is the very slow rate of binding of N_2O, which, according to computational studies, involves formation of a low-spin adduct. The reasons for the slow binding are attributed to rearrangements that occur during what is in effect an oxidative addition reaction. These are discussed further under the individual substrate sections.

4.2. PhNO. This reagent has the slowest rate of OAT in part because the N−O BDE is highest for it. The rate of binding occurs reasonably fast at low temperatures, but OAT does not occur until near 0 °C. PhNO is isoelectronic with O_2 but unlike O_2 its ground state is a singlet. NMR studies show that the **1**−ONPh adduct is low spin, as are both the η^1 and η^2 binding modes of O_2.[41] However, unlike O_2, which is considerably more stable in its η^2-binding form, computational studies show that for PhNO, the η^1 is more stable than the η^2-binding, presumably for steric reasons. The enthalpy of binding of PhNO to form η^1-**1**−ONPh (−54 kcal mol^{-1}) compares with that of η^2-**1**−O_2 (−75 kcal mol^{-1}).

The most probable mode of OAT is decomposition of the low-spin complex **1**−ONPh to generate free ^{3}NPh and **1**≡O in a unimolecular reaction. Due to the high heat of binding of PhNO and concomitant stability of **1**−ONPh, even generation of the lower energy (by 18 kcal mol^{-1}) triplet nitrene is endothermic as an elementary step by about 8 kcal mol^{-1}, and the reaction is driven forward only by trapping of the nitrene. There are therefore two MECP's in this reaction, a cross over from the triplet **1** and singlet PhNO to form the singlet complex in ligand binding, followed by OAT, which involves reverting back to a triplet state of bound **1**−ONPh, which then eliminates ^{3}NPh and singlet **1**≡O. The observed enthalpy of activation for actual OAT (19 kcal mol^{-1}), as well as some qualitative trapping experiments are all consistent with this mechanism; however, it will not be proven until spectroscopic observation or other incontrovertible evidence is found. Nonetheless, the slowest nature of PhNO for OAT among all the XNO reagents studied here seems to be the consequence of the high stability of the adduct as well as the extrusion of the unstable triplet nitrene.

4.3. PyO. PyO has the fastest rate of binding of all the substrates studied here. Furthermore, ligand binding was essentially irreversible at low temperature for the high-spin complex formed. Due to the basicity of pyridine, the electron density on the donor O atom of PyO would be expected to be the most basic, and the stability of high-spin O bonded donors would be expected to be in the order PyO > MesCNO > N_2O. The NHC adducts of MesCNO and N_2O would be expected to also have increased electron density on the donor O atom compared with the free ligands. Despite rapid and irreversible adduct formation and a lower or similar N−O BDE than the NHC adducts of MesCNO and N_2O, respectively, PyO underwent relatively slow OAT, and the activation barrier for k_2 (15 kcal mol^{-1}) is high enough that it yielded a readily separable two-step process. A plausible explanation is that there are no π^* orbitals available to accept electron density and that this forces a higher energy MECP involving a larger geometric rearrangement to involve instead the σ^* orbitals. While intuitively reasonable, this premise will be tested by more detailed computational studies in progress.

4.4. N_2O. Due to its importance as a ligand and the fact that it undergoes dinuclear activation, N_2O is discussed in more detail. The pioneering work of Taube's group[5] had shown

much earlier that the preformed complex $(NH_3)_5RuN_2O^{2+}$ underwent rapid OAT with Cr^{2+} but that reaction between Cr^{2+} and free N_2O required months under similar conditions. This sets the precedent for dinuclear OAT involving nitrous oxide between different metallic fragments. Chang and co-workers[8] have reported the first crystal structure of a nitrous oxide complex $(tpa^{Mes})VNNO$, which might be expected to be similar in nature to any intermediate complex formed between N_2O and **1**. The presence of the coordinating base in the $(tpa^{Mes})V$ system results in formation of a linear high-spin complex. In contrast, DFT studies done here suggest that for **1**−NNO the binding should be low spin with a doubly bent N_2O group. Computational studies by Caulton and co-workers have suggested a new binding form for N_2O as a dianion, and that is also in keeping with our calculated structure of **1**═N—N═O. Binding of N_2O to **1** through O is thermochemically unfavorable (ΔH_{bind} = 12.1 kcal mol^{-1}, Table 1), and also the high-spin N-bound adduct is unstable (ΔH_{bind} = 3.1 kcal mol^{-1}, Table 1). Likewise, the diamagnetic V(V) complex is computed to be of marginal stability. The relatively slow nature of binding at high temperatures is in keeping with the fact that binding is a reversible process to yield the low-spin **1**═N—N═O adduct. Once formed, the key factor determining the fate of the nitrosoimido species is the k_{-1}/k_2 ratio of its dissociation back to **1** and N_2O versus its rate of trapping by free **1** to yield a bridging N_2O intermediate complex **1**═N—N═O−**1**, which subsequently fragments with a low barrier to **1**≡O and **1**−NN, which rapidly loses N_2 to yield the observed products. The proposed termolecular reaction for N_2O is in keeping with recent calculations of Lin et al.[6] who have concluded that OAT studied for Cp_2V by Bergman and co-workers actually occurs by initial binding through N of N_2O to one V center, followed by essentially barrierless OAT to a second V center. The derived reaction profile for OAT between N_2O and 2 mol of **1** is shown in Figure 12.

The reaction profile is computed based on the experimental enthalpies of activation for k_1 (6.3 kcal mol^{-1}), as well as k_{-1} (13 kcal mol^{-1}) and k_2 (3.0 kcal mol^{-1}). The equilibrium binding enthalpy (determined from k_1/k_{-1} at various temperatures) is computed to be −6.7 kcal mol^{-1}. This analysis shows that there is a much greater enthalpy of activation for the k_{-1} step than for the k_2 step. However, the entropy change for the k_{-1} step (−6 cal mol^{-1} K^{-1}) is less negative than that associated with the k_2 step (−27 cal mol^{-1} K^{-1}). Thus, as the temperature is raised, k_{-1} will increase much more rapidly than k_2. This has the consequence of moving the transition state in the reaction from TS1 to TS2 in Figure 12 with the counterintuitive result that third-order kinetics is followed at high T and second-order at low T. The slowness of the reaction, compared with other binding reactions, is reflected primarily in the unfavorable entropy of activation.

It is of interest to compare reaction of 2 mol of **1** with N_2O to the quite different results when Mo rather than V is the metal center as shown in eq 15 where N_2O undergoes dinuclear

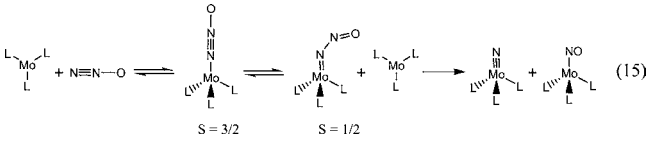

(15)

activation[42] with cleavage of the N−N rather rather than the N−O bond. The rate-determining step in dinuclear cleavage of

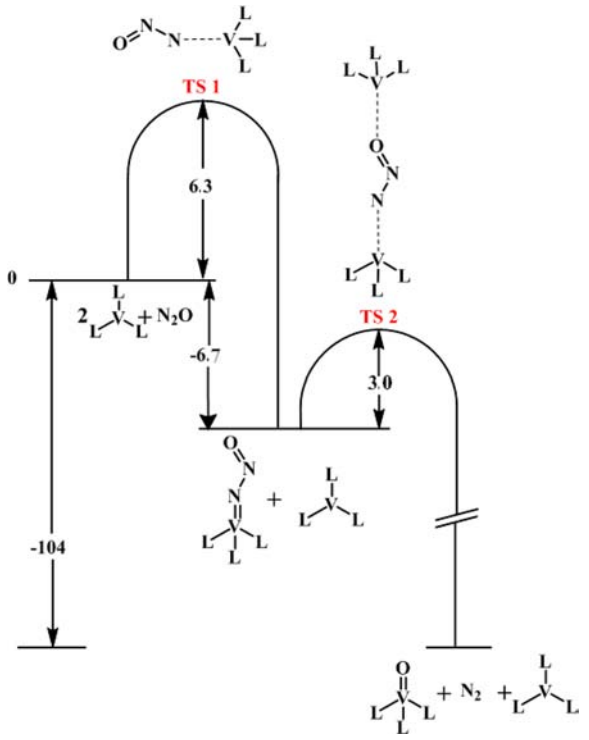

Figure 12. Potential energy (kcal mol^{-1}) diagram for reaction 2**1** + N_2O → **1**≡O + **1** + N_2 by dinuclear OAT. At low T, the rate-determining step occurs at ligand binding (TS1) and the reaction obeys the rate law $dP/dt = k_1[\mathbf{1}][N_2O]$. At high temperatures, the rate-determining step occurs at formation of the dinuclear complex **1**═N—N═O−**1** (TS2), and the reaction obeys the rate law $dP/dt = (k_1k_2/k_{-1})[\mathbf{1}]^2[N_2O]$. See text for additional discussion.

the N−N bond of N_2O by $Mo(N[t\text{-}Bu]Ar)_3$ was initial binding to form the highly potent nitrosylating agent $ONNMo(N[t\text{-}Bu]Ar)_3$. Activation parameters for the rate-determining step were $\Delta H^{\ddagger}$ = 9.7 kcal mol^{-1} and $\Delta S^{\ddagger}$ = −24 kcal mol^{-1}. Generation of free NO,[43] though energetically allowed, was excluded based on competition and trapping experiments.

4.5. MesCNO. The rate of reaction of MesCNO is intermediate between that of the two NHC adducts studied (IPr/N_2O and MesCNO/SIPr), which are discussed together in the next section. MesCNO most closely resembles N_2O in terms of structure and bonding, and yet it reacts much faster. This is attributed to the fact that while both ligands are computed to bind in an endothermic reaction to **1**, coordination of MesCNO (4.5 kcal mol^{-1}) is less endothermic than the O-binding of N_2O (12.1 kcal mol^{-1}). In reaction of **1** with MesCNO, it is postulated that k_{-1} plays a possible role in slowing down the reaction. Provided $k_{-1} \gg k_2$, the net rate for OAT via a steady-state mechanism becomes $k_{obs} = k_1k_2/k_{-1} = K_{eq}k_2$. Experimental plots of k_{obs} versus MesCNO concentration, particularly at higher temperatures, appear to give nonzero intercepts suggesting that k_{-1} may play a role in the kinetic scheme.

4.6. IPr/N_2O and SIPr/MesCNO. As shown in Table 1, DFT results show enhanced enthalpies of binding of the NHC adducts of N_2O and MesCNO compared with the parent substrates. This is presumably due to increased electron density on the terminal O atom due to inductive effects from the highly basic NHCs. Computations predict that the adducts between IPr/N_2O and **1** should be energetically similar for both low- and high-spin states using a truncated ligand system (IMe

dx.doi.org/10.1021/ja405395z | J. Am. Chem. Soc. 2013, 135, 11357−11372

rather than IPr) suggesting that both species may in principle coexist in equilibrium. The TD DFT computed UV−vis spectrum for the singlet **1**−ON_2/IMe adduct (See Supporting Information) is in good agreement with the actual spectral data of the intermediate detected in stopped flow experiments. For SIPr/MesCNO, DFT calculations predict that a high-spin triplet state is most stable.

Global modeling of the IPr/N_2O kinetic data yielded activation parameters for ligand binding (k_1) of $\Delta H_1^{\ddagger}$ = 5.6 ± 0.4 kcal mol^{-1} and $\Delta S_1^{\ddagger}$ = −18 ± 2 cal mol^{-1} K^{-1} and for OAT (k_2) of $\Delta H_2^{\ddagger}$ = 13 ± 1 kcal mol^{-1} and $\Delta S_2^{\ddagger}$ = 1 ± 2 cal mol^{-1} K^{-1}. These data can be compared with SIPr/MesCNO: $\Delta H_1^{\ddagger}$ = 4.9 ± 0.4 kcal mol^{-1} and $\Delta S_1^{\ddagger}$ = −19 ± 2 cal mol^{-1} K^{-1} for ligand binding and $\Delta H_2^{\ddagger}$ = 9.3 ± 0.3 kcal mol^{-1} and $\Delta S_2^{\ddagger}$ = −9 ± 1 cal mol^{-1} K^{-1} for OAT. It is worth noting that MesCNO reacts faster than N_2O and that order is retained in the NHC adducts as well.

An unanswered question in these complex systems is at what point do they fragment to smaller pieces. This is illustrated for SIPr/MesCNO with the two possible OAT pathways shown in eqs 16 and 17.

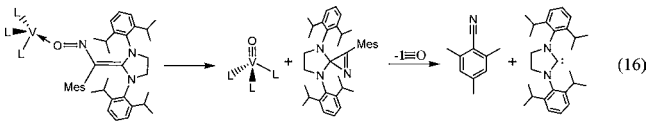

(16)

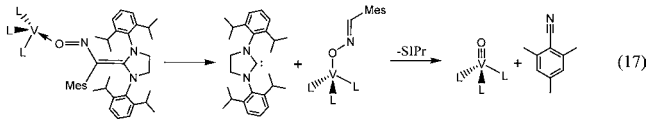

(17)

As shown in eq 16, actual OAT could occur with dissociation of an intact SIPr/MesCN fragment, which would subsequently dissociate rapidly to MesCN and SIPr.[44] A second possibility as shown in eq 17 is that the NHC would initially dissociate from the bound adduct, followed by OAT and dissociation of MesCN. In this second scenario, the NHC could be viewed as a catalyst that delivers MesCNO in a configuration more suitable for OAT and then dissociates. The accelerating effect of NHC coordination suggests their possible utility as catalysts for substrate activation.[45] That acceleration is attributed to both increased favorability of ligand binding (k_1/k_{-1}) and also the accessibility of π^* orbitals to participate in the OAT (k_2) step.

4.7. dbabhNO. The net rate of reaction of dbabhNO is intermediate between SIPr/MesCNO and IPr/N_2O with the important difference that no intermediate adduct is detected. This implies that the steady-state approximation is valid, that intermediates decay at about the same rate as they are produced. The fact that the overall reaction is relatively fast and near the range expected for rates of ligand binding (unlike MesCNO) implies a more efficient OAT than that for MesCNO. It can be postulated that $k_1 > 1.8 \times 10^3$ M^{-1} s^{-1} for dbabhNO at −62 °C. For IPr/N_2O, which reacts more slowly than dbabhNO, k_1 = 785 ± 54 M^{-1} s^{-1} and k_2 = 0.308 ± 0.014 s^{-1} at −62 °C. It is clear that k_1 is larger for dbabhNO and also that the net rate of reaction is faster. Since intermediate does not build up, it can be concluded that k_2 must also be greater for dbabhNO than for IPr/N_2O.

The extremely weak N−O BDE of 10 kcal mol^{-1} based on thermochemical measurements would suggest extremely facile OAT to **1** based on thermodynamics alone. However, the thermodynamic BDE is based on full fragmentation of dbabhNO to O, anthracene, and N_2 and it is gaining the resonance energy of anthracene and stability of N_2, which give this stable compound such a low formal BDE. The initial stages of OAT, however, need not involve complete fragmentation of the molecule. As discussed above for SIPr/MesCNO, following spin pairing dissociation could conceivably proceed by a rapid two-step process as shown in eq 18:

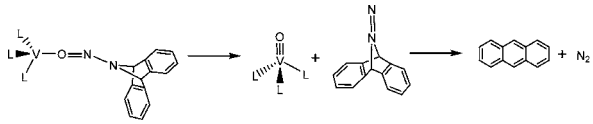

(18)

Such a two-step process would mean that not all of the energy of the reaction is released in step 1 because generation of anthracene and dinitrogen in step 2 will be exothermic. This could conceivably be rapid even on the stopped flow time scale. Based on thermochemistry alone, dbabhNO would be expected to be the most rapid OAT reagent. It is possible that the fact that it is not the fastest is due simply to a low rate of binding and that in fact OAT is "instantaneous" once bound. More detailed experimental and computational work on dbabhNO is in progress.

5. CONCLUSION

The original goal of this work was to answer the simple question of whether adducts of MesCNO and N_2O reacted faster, slower, or at the same rate as the unbound substrates. Fortuitous kinetic results allowed us to take a more complete view of OAT in the XNO series. While the facts lie in the rate and activation parameters themselves, the mechanistic picture that evolves is not as simple as the authors anticipated. It seems clear, as pointed out by other workers in this area, that detailed mechanistic understanding must necessarily involve a complete picture involving binding, spin pairing, electron transfer, bond cleavage, and fragment elimination. These need not occur in that order and may appear in different steps for different substrates. For example, PhNO undergoes binding and electron transfer and spin pairing in one step; in contrast PyO simply binds in a high-spin state and later undergoes electron transfer and spin pairing before going onward to complete OAT. It is tempting to state that initial binding is the key factor in the OAT process in most cases, but that hides the fact that binding may be different for different substrates. The main difference in the rate of binding of PyO and N_2O is the entropy of activation to form the complex. Surprisingly, the enthalpies of activation overlap within experimental error. This may relate to the transition state for binding being relatively distant from the V center for the high-spin PyO adduct, which remains paramagnetic, compared with N_2O, which is computed to yield a low-spin complex in which oxidation of **1** has already occurred and which is formulated as a bent diamagnetic complex **1**≡N−N=O. This may require a much more constricted reaction pathway despite the fact that both are "ligand binding" events. More detailed computational and additional experimental work is in progress to further define this critical process. The current work presents the experimental backdrop for those studies, but has also generated several surprising results:

a. The V−O bond in **1**≡O (BDE = 154 kcal mol^{-1}) is strong enough for **1** to cleave all NO bonds except for NO itself in a direct reaction.
b. Rates of ligand binding play a role in the overall OAT process, but it is complex since both low-spin and

dx.doi.org/10.1021/ja405395z | J. Am. Chem. Soc. 2013, 135, 11357−11372

high-spin adducts occur depending upon XNO. Crossing may occur before or after adduct formation. In some cases, ligand binding is the rate-determining step; in some cases, OAT from the bound complex is the rate-determining step.

c. The relatively slow rate of OAT of PyO is attributed to slow conversion of the high-spin **1**−OPy adduct to a low-spin form. The lack of an available NO π^* orbital may force a more bent transition state than for other adducts.
d. The slow rate of OAT for PhNO, despite detection of a stable low-spin adduct, is due to the stability of the adduct and a relatively large enthalpy of activation for expulsion of the unstable ^{3}NPh fragment.
e. No simple correlation was found between BDE and rates of OAT. Despite a formally stronger N−O BDE and increased steric hindrance, the adducts SIPr/MesCNO and IPr/N_2O undergo more rapid OAT to the bulky complex **1** than MesCNO and N_2O themselves. This is attributed primarily to electronic factors making available an NO π^* orbital.
f. OAT with N_2O occurs in a termolecular process involving reversible formation of an N-bonded adduct **1**−NNO, which then forms **1**−NNO−**1** prior to OAT. The rate-determining step changes as a function of temperature due to the activation parameters for the individual binding and OAT step involved as discussed in the text.
g. The unique OAT reagent dbabhNO undergoes rapid OAT with **1** and its N−O BDE of 10 kcal mol^{-1} implies that thermochemically generation of a ^{3}O atom from this stable reagent is thermodynamically favored at room temperature.
h. It appears that bent structures such as SIPr/MesCNO, IPr/N_2O, and **1**−N_2O undergo more rapid OAT than linear precursors such as N_2O and MesCNO. The enhanced rate of OAT for the NHC bound complexes may lead to their utilization as accelerants in some reactions in designed complexes.

Additional work is in progress to further map the kinetics, thermodynamics, and complete reaction profile for OAT involving the N−O bond and transition metals of potential catalytic utility.

■ ASSOCIATED CONTENT

Supporting Information

Experimental details and supporting data as mentioned in the text. This material is available free of charge via the Internet at http://pubs.acs.org.

■ AUTHOR INFORMATION

Corresponding Author

elena.rybak-akimova@tufts.edu; manuel.temprado@uah.es; ccummins@mit.edu; captain@miami.edu; c.hoff@miami.edu.

Notes

The authors declare no competing financial interest.

■ ACKNOWLEDGMENTS

The authors dedicate this paper to Professor Robert E. Gawley (1948−2013). This material is based upon work supported by (a) the National Science Foundation under Grants CHE-1111357 (C.C.C.), CHE-0615743 (C.D.H.), CHE-0750140 (E.V.R.-A.), and CRIF-0639138 (E.V.R.-A.), (b) the Spanish Ministry of Economy and Competitiveness (MINECO) under Grant CTQ2012-36966 (M.T.), (c) the Natural Sciences and Engineering Research Council of Canada postdoctoral fellowship (A.F.C.), and (d) a GAANN Fellowship (T.D.P.).

■ REFERENCES

(1) Abu-Omar, M. M. in *Physical Inorganic Chemistry. Reactions, Processes, and Applications*; Bakac, A., Ed.; Wiley: Hoboken, NJ, 2010; pp 75−108.
(2) Ravishankara, A. R.; Daniel, J. S.; Portmann, R. W. *Science* **2009**, *326*, 123−125.
(3) Zhang, F.; Chen, X.; Zhuang, J.; Xiao, Q.; Zhong, Y.; Zhu, W. *Catal. Sci. Technol.* **2011**, *1*, 1250−1255.
(4) Tolman, W. B. *Angew. Chem., Int. Ed.* **2010**, *49*, 1018−1024.
(5) Armor, J. N.; Taube, H. *J. Am. Chem. Soc.* **1971**, *93*, 6476−6480.
(6) (a) Yu, H.; Jia, G.; Lin, Z. *Organometallics* **2009**, *28*, 1158−1164. (b) Yu, H.; Jia, G.; Lin, Z. *Organometallics* **2008**, *27*, 3825−3833. (c) Yu, H.; Jia, G.; Lin, Z. *Organometallics* **2007**, *26*, 6769−6777.
(7) Fan, H.; Caulton, K. G. *Polyhedron* **2007**, *26*, 4731−4736.
(8) Piro, N. A.; Lichterman, M. F.; Harman, W. H.; Chang, C. J. *J. Am. Chem. Soc.* **2011**, *133*, 2108−2111.
(9) (a) Jana, A.; Roesky, H. W.; Schulzke, C. *Dalton Trans.* **2010**, *39*, 132−138. (b) Demir, S.; Montalvo, E.; Ziller, J. W.; Meyer, G.; Evans, W. J. *Organometallics* **2010**, *29*, 6608−6611. (c) Harrold, N. D.; Waterman, R.; Hillhouse, G. L.; Cundari, T. R. *J. Am. Chem. Soc.* **2009**, *131*, 12872−12873. (d) Harman, W. H.; Chang, C. J. *J. Am. Chem. Soc.* **2007**, *129*, 15128−15129. (e) Kaplan, A. W.; Bergman, R. G. *Organometallics* **1997**, *16*, 1106−1108.
(10) (a) Laplaza, C. E.; Odom, A. L.; Davis, W. M.; Cummins, C. C.; Protasiewicz, J. D. *J. Am. Chem. Soc.* **1995**, *117*, 4999−5000. (b) Cherry, J. P. F.; Johnson, A. R.; Baraldo, L. M.; Tsai, Y. C.; Cummins, C. C.; Kryatov, S. V.; Rybak-Akimova, E. V.; Capps, K. B.; Hoff, C. D.; Haar, C. M.; Nolan, S. P. *J. Am. Chem. Soc.* **2001**, *123*, 7271−7286.
(11) Parmon, V. N.; Panov, G. I.; Uriarte, A.; Noskov, A. S. *Catal. Today* **2005**, *100*, 115−131.
(12) Schultz, B. E.; Holm, R. H. *Inorg. Chem.* **1993**, *32*, 4244−4248.
(13) McPherson, L. D.; Drees, M.; Khan, S. I.; Strassner, T.; Abu-Omar, M. M. *Inorg. Chem.* **2004**, *43*, 4036−4050.
(14) (a) Veige, A. S.; Slaughter, L. M.; Wolczanski, P. T.; Matsunaga, N.; Decker, S. A.; Cundari, T. R. *J. Am. Chem. Soc.* **2001**, *123*, 6419−6420. (b) Veige, A. S.; Slaughter, L. M.; Lobkovsky, E. B.; Wolczanski, P. T.; Matsunaga, N.; Decker, S. A.; Cundari, T. R. *Inorg. Chem.* **2003**, *42*, 6204−6224.
(15) Crestoni, M. E.; Fornarini, S.; Lanucara, F.; Warren, J. J.; Mayer, J. M. *J. Am. Chem. Soc.* **2010**, *132*, 4336−4343.
(16) Fortner, K. C.; Laitar, D. S.; Muldoon, J.; Pu, L.; Braun-Sand, S. B.; Wiest, O.; Brown, S. N. *J. Am. Chem. Soc.* **2007**, *129*, 588−600.
(17) Vasbinder, M. J.; Espenson, J. H. *Organometallics* **2004**, *23*, 3355−3358.
(18) Park, J.; Morimoto, Y.; Lee, Y. M.; Nam, W.; Fukuzumi, S. *J. Am. Chem. Soc.* **2011**, *133*, 5236−5239.
(19) Keith, J. M.; Tomić, Z. D.; Zarić, S. D.; Hall, M. B. *J. Mol. Catal. A: Chem.* **2010**, *324*, 15−23.
(20) (a) O'Reilly, M. E.; Del Castillo, T. J.; Abboud, K. A.; Veige, A. S. *Dalton Trans.* **2012**, *41*, 2237−2246. (b) O'Reilly, M. E.; Ghiviriga, I.; Abboud, K. A.; Veige, A. S. *J. Am. Chem. Soc.* **2012**, *134*, 11185−11195.
(21) Cai, X.; Majumdar, S.; Fortman, G. C.; Frutos, L. M.; Temprado, M.; Clough, C. R.; Cummins, C. C.; Germain, M. E.; Palluccio, T.; Rybak-Akimova, E. V.; Captain, B.; Hoff, C. D. *Inorg. Chem.* **2011**, *50*, 9620−9630.
(22) Tskhovrebov, A. G.; Solari, E.; Wodrich, M. D.; Scopelliti, R.; Severin, K. *Angew. Chem., Int. Ed.* **2012**, *51*, 232−234.
(23) Tskhovrebov, A. G.; Solari, E.; Wodrich, M. D.; Scopelliti, R.; Severin, K. *J. Am. Chem. Soc.* **2012**, *134*, 1471−1473.

(24) More detailed computational, as well as additional experimental, studies of OAT between XNO and different metal complexes are in progress.
(25) Ruppa, K. B. P.; Desmangles, N.; Gambarotta, S.; Yap, G.; Rheingold, A. L. *Inorg. Chem.* **1997**, *36*, 1194−1197.
(26) The structure of the analogous **1**≡S has been reported: Brask, J. K.; Dura-Vila, V.; Diaconescu, P. L.; Cummins, C. C. *Chem. Commun.* **2002**, 902−903.
(27) Carpino, L. A.; Padykula, R. E.; Barr, D. E.; Hall, F. H.; Krause, J. G.; Dufresne, R. F.; Thoman, C. J. *J. Org. Chem.* **1988**, *53*, 2565−2572.
(28) (a) Fickes, M. G.; Davis, W. M.; Cummins, C. C. *J. Am. Chem. Soc.* **1995**, *117*, 6384−6385. (b) Proulx, G.; Bergman, R. G. *J. Am. Chem. Soc.* **1995**, *117*, 6382−6383.
(29) Luo, Y. R. *Handbook of Bond Dissociation Energies in Organic Compounds*; CRC Press: Boca Raton, FL, 2003.
(30) http://webbook.nist.gov.
(31) It is standard to use $T\Delta S \approx 10$ kcal mol^{-1} at rt for each gain in total number of particles of products minus reactants, see: Page, M. I. *Angew. Chem., Int. Ed. Engl.* **1977**, *16*, 449−459. In reaction 8, since there is a two particle advantage for the products, the favorable $T\Delta S$ term of approximately −20 kcal/mol will overcome the ΔH of approximately 10 kcal/mol to yield an estimated ΔG on the order of -10 ± 5 kcal/mol.
(32) Gritsan, N. P.; Platz, M. S. *Chem. Rev.* **2006**, *106*, 3844−3867.
(33) (a) Platz, M. S. *Acc. Chem. Res.* **1995**, *28*, 487−492. (b) Borden, W. T.; Gritsan, N. P.; Hadad, C. M.; Karney, W. L.; Kemnitz, C. R.; Platz, M. S. *Acc. Chem. Res.* **2000**, *33*, 765−777.
(34) (a) Liang, T. -Y.; Schuster, G. B. *J. Am. Chem. Soc.* **1987**, *109*, 7803−7810. (b) Takaoka, A.; Moret, M.-E.; Peters, J. C. *J. Am. Chem. Soc.* **2012**, *134*, 6695−6706.
(35) For example, a dinuclear reaction with a rate-limiting mononuclear first step between an activated form of **1**−ONPh and **1**−ONPh to yield PhNNPh and two **1**≡O or an activated form of **1**−ONPh and **1** to yield **1**≡O and **1**═NPh.
(36) In most systems, the change in absorbance at λ = 453 nm (λ_{max} for **1**≡O) was followed. For reactions with IPr/N_2O, however, the absorbance was too intense in that region of the spectrum. Analysis of data at 453 nm, when possible, was in agreement with analysis at λ = 725 nm.
(37) Moerdyk, J. P.; Bielawski, C. W. *J. Am. Chem. Soc.* **2012**, *134*, 6116−6119.
(38) The most commonly cited O═M bond strength measured for a complex in solution is that of Watt, G. D.; McDonald, J. W.; Newton, W. E. *J. Less-Common Met.* **1977**, *54*, 415.
(39) Carreon-Macedo, J. L.; Harvey, J. N. *J. Am. Chem. Soc.* **2004**, *126*, 5789−5797.
(40) Temprado, M.; McDonough, J. E.; Mendiratta, A.; Tsai, Y. C.; Fortman, G. C.; Cummins, C. C.; Rybak-Akimova, E. V.; Hoff, C. D. *Inorg. Chem.* **2008**, *47*, 9380−9389.
(41) Cozzolino, A. F.; Tofan, D.; Cummins, C. C.; Temprado, M.; Pallucio, T. D.; Rybak Akimova, E. V.; Majumdar, S.; Cai, X.; Captain, B.; Hoff, C. D. *J. Am. Chem. Soc.* **2012**, *134*, 18249−18252.
(42) Cherry, J. P. F.; Johnson, A. R.; Baraldo, L. M.; Tsai, Y. C.; Cummins, C. C.; Kryatov, S. V.; Rybak-Akimova, E. V.; Capps, K. B.; Hoff, C. D.; Haar, C. M.; Nolan, S. P. *J. Am. Chem. Soc.* **2001**, *123*, 7271−7286.
(43) Khoroshun, D. V.; Musaev, D. G.; Morokuma, K. *Organometallics* **1999**, *18*, 5653−5660.
(44) Some NHC/nitrile adducts have been reported to be stable; no adduct exists between MesCN and SIPr to the authors' knowledge.
(45) Enders, D.; Niemeier, O.; Henseler, A. *Chem. Rev.* **2007**, *107*, 5606−5655.